SEMMELWEIS EGYETEM

DOKTORI ISKOLA

Ph.D. értekezések

3282.

BORBÁS BENCE

A gyógyszerészeti tudományok korszerű kutatási irányai

című program

Programvezető: Dr. Antal István, egyetemi tanár

Témavezető: Dr. Antal István, egyetemi tanár

Additive Manufacturing Applications in Pharmaceutical Sciences: osmotic delivery modular tablet and dry media grinding.

PhD thesis

Bence Borbás

Semmelweis University Doctoral School

Pharmaceutical Sciences and Health Technologies Division

Supervisor: Dr. István Antal, PhD

Official reviewers: Dr. Zoltán Ujhelyi, PhD
Dr. Imre J. Barabás, PhD

Head of the Complex Examination Committee:
Dr. Éva Szökő, D.Sc

Members of the Complex Examination Committee:
Dr. Miklós Vecsernyés, Ph.D
Dr. László Tóthfalusi, DSC

Budapest
2025

Table of contents

List of abbreviations

Abbreviated form	**The meaning of the abbreviated term**
3D	3 dimensional
AM	Additive manufacturing
API	Active pharmaceutical ingredient
CA	Cellulose acetate
CAD	Computer-aided design
DSC	Differential scanning calorimeter
EOP	Elementary osmotic pump
FDM	Fused deposition modelling
GIT	Gastro-intestinal tract
GLY	Glycerol
HPMC	hydroxy propyl methyl cellulose (Hypromellose)
IR	Immediate release
OROS	Osmotic release oral system
PALS	Positron annihilation lifetime spectroscopy
pcs	pieces
PG	Propylene glycol
Ph. Eur.	European Pharmacopoeia
RPM	Revolutions per minute
RSD	Relative standard deviation
SD	Standard deviation
SEM	Scanning electron microscopy
SLA	Stereolithography
USP	United States Pharmacopoeia
UV	Ultraviolet

1. Introduction

1.1. The additive manufacturing (AM)

1.1.1. The applicability of 3D printing

The interest in 3D printing is increasing due to its potential applications in personalized medicine [1]. Because of the innovative and flexible nature of the tool, it can be used in many areas of pharmaceutical research, manufacturing and drug therapies. Furthermore, AM is considered a cost-effective [2], sustainable and environmentally friendly option for fabricating different drug delivery systems, or tools for the pharmaceutical industries [3].

With this method, the required dose of the active pharmaceutical ingredient (API) and the shape of different dosage forms can be adjusted according to the patients' needs [4]. The unique performance of the additively manufactured dosage forms can be especially important in the case of paediatrics [5] and geriatrics [6], and for those patients who have metabolic diseases [7]. 3D printing has the possibility to print porous and loose tablets, which can help patients with dysphagia to swallow the tablet [8]. Because of the aforementioned possibilities of the AM, the patients are shown better compliance, which facilitates better therapeutic results for healthcare professionals [9].

1.1.2. The design of the printlets

As the first step of the 3D printing process in case of all types of printing methods, is that the model of the printlet must be created with a 3D designing software, and the created model has to be sliced into well-defined horizontal slices in a specific slicer software before the printing [10]. As the result of the slicing, an SL1S file is obtained which contains the exact printing parameters: the printing material, the layer height or resolution, and the coordinates in the 3 dimensions, the printer is going to follow to build up the structure. The sliced file contains other pieces of information as well, which are specific to the exact 3D printing method, like the initial exposure time, and the exposure time in the case of stereolithography (SLA) printing and the temperature of the extruder, the temperature of the printer bed, and the infill percentage in the instance of the fused deposition modelling (FDM) printing[10, 11]. After slicing the 3D model, the sliced file is transported into the 3D printer, where the printer builds up the printlet layer by layer [12].

1.1.3. Additive manufacturing methods

Additive manufacturing is a group with a vast number of individual 3D printing methods.

FDM printing is a common method where a thermoplastic filament is melted during the fabrication process and the melted filament is left the extruder through a nozzle, and is added on the previous layers, that is placed on the printer's bed in the prior printing steps. This is considered a simple method with a wide variety of biocompatible and biodegradable printing materials [13, 14]. The two main limitations of the method are its high printing temperature, because most of the active substances cannot tolerate the high temperature (between 150 and 250 °C), which is essential for melting the filaments, also the resolution of the method is considered limited [13, 15].

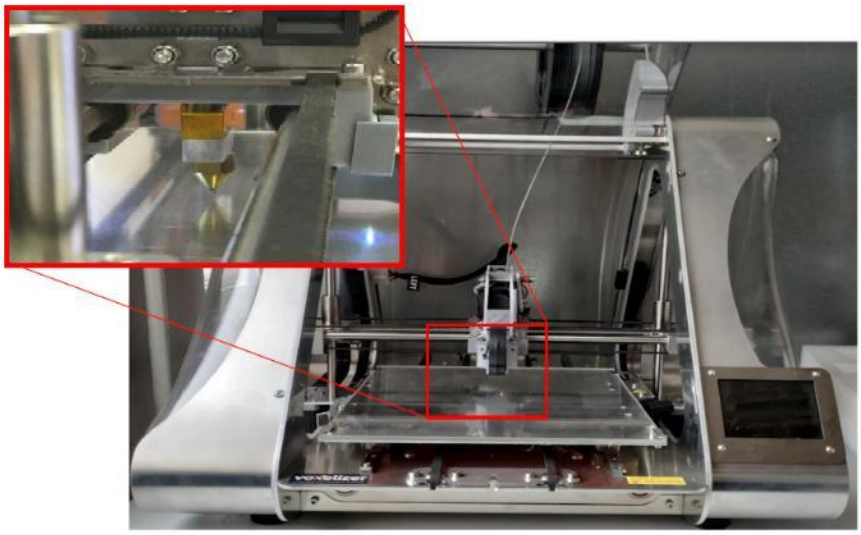

Figure 1: FDM printer (Zmorph FDM printer)

Another well-established method of the AM is the SLA printing [16]. In the instance of the SLA method, the layers are solidified together due to the photopolymerization of the printing resin that is filled into the printer's resin tank prior to the beginning of the printing. Ultraviolet (UV) light is the most commonly used initiation source; however, lights with various wavelengths can also be employed to form a crosslinked matrix structure [17]. After the light exposure of each layer, the printing platform is moved upwards to create space for the next layer [11]. The main advantages of the method are its high resolution, and its high printing speed compared to the FDM method. The SLA method is suitable for the utilization of thermosensitive APIs and

excipients because of the lack of heat transfer [18]. The main challenges of the SLA printing are the stability and safety issues, which are based on the materials that are used in the fabrication [19].

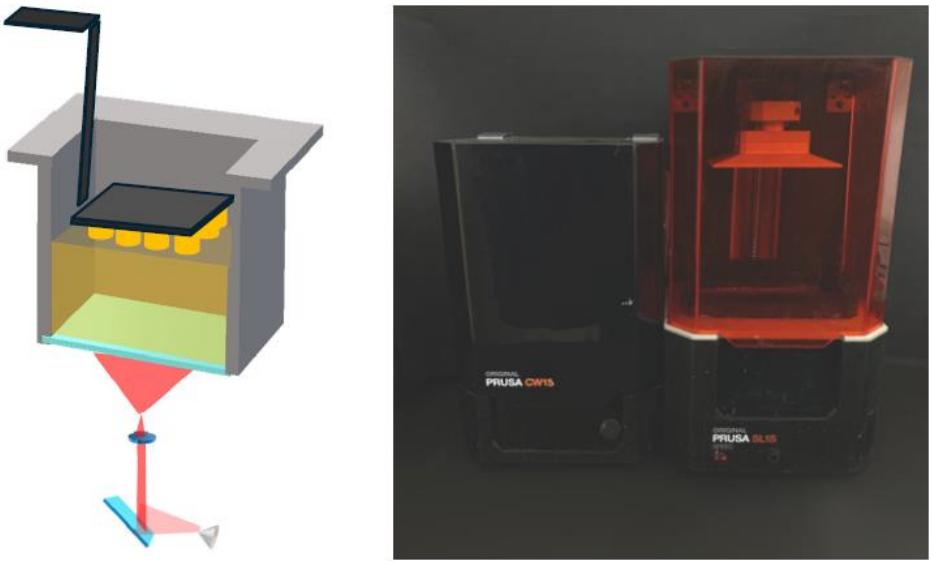

Figure 2: The schematic image and a picture of an SLA printer[11]

In the researches that is presented in the current thesis the FDM and the SLA methods is considered as flexible tools, however, because of the high resolution of the SLA printing, that is required to print out spherical milling balls in different sizes, and parts of an osmotic drug delivery system, where the elements were assembled akin to Lego® blocks, where the small details of the delivery system can influence the controlled and programmed delivery of the API.

1.1.4. Modular, controlled systems with 3D printing

Preparing pharmaceutical dosage forms with a modular structure with AM is a relatively new field in pharmaceutical research. Pereira et al designed a complex structure, so-called “polypill” capsule, which contained two modular capsule skeletons with four compartments. The controlled and targeted drug delivery was achieved with the modification of the parameters of the different modules [20]. Lu et al designed multi-compartment tablets that contained three different antiviral model drugs, each loaded into different layers of the modular system. The dissolution of the drugs from the different layers happened with different drug release rates, which enables the personalization of the drug delivery [21]. Meleocchi et al were constructed a multicompartment modular device, where the matching modular units are assembled with different wall compositions

akin to Lego® blocks. The pulsatile release of the caffeine model drug was experienced, which was influenced by the elements that were used to assemble [22]. Govender et al were designed a modular product which contained two submodules, printed out with FDM technology. The fabrication of this modular drug delivery system showed that the drug release can be flexible and variable by the variation of the submodules [23]. Based on these previous studies, the attention towards the flexible, modular approach of the AM has grown; fabrication of a modular push-pull type osmotic release drug delivery system, which was one of the aims of the current research, is considered a novel approach.

1.2. Osmotic Release Oral System (OROS)

1.2.1. Drug release profiles

The significance of pharmaceutical dosage forms with modified drug release has become increasingly recognised in recent decades. The current thesis concentrates on the tablet dosage form as a solid, single-dose formulation, with a declared content of APIs. The drug release profile of the dosage form could be varied. In the case of the immediate release formulations (IR), the release of the active substance is not modified by any formulation techniques or by any changes in the composition. In this case, the drug release is started after the intake, and the whole amount of the API is released after a couple of hours. This results in a well-defined maximum peak in the blood concentration graph of the drug, with a rapid decrease of the concentration after it reaches its maximum in time [24].

In the instance of formulations with modified release, the dissolution of the drug substance was altered during the formulation with specific techniques or special composition to avoid the cyclical fluctuation of the active substance concentration [25]. Delayed, pulsatile and extended release are the variations of the modified API release [26]. If a formulation has delayed drug release, the dissolution of the API is started after a lag-time period. This type of release is used when the API has to be transferred to the optional phase of the gastrointestinal tract, where the conditions are safe and optimal for the API to absorb [27]. Pulsatile release of the drug means that the total amount of the active substance is released in well-defined doses separated in time as the pathophysiological need of the disease, or certain vital functions change intermittently [28]. In the instance of extended release formulations, the API is released from the dosage form over an extended period of time after administration [29]. The types of active

substance release are shown in Figure 3. OROS are part of the extended-release formulations. In the case of OROS formulations, the driving force of the controlled release of the active substance is the osmotic pressure difference between the two sides of a semipermeable membrane. This osmotic gradient results water diffusion into the osmotic core through the semipermeable membrane, and results an increased hydrostatic pressure in the system, which presses out the API through a drug delivery orifice [30].

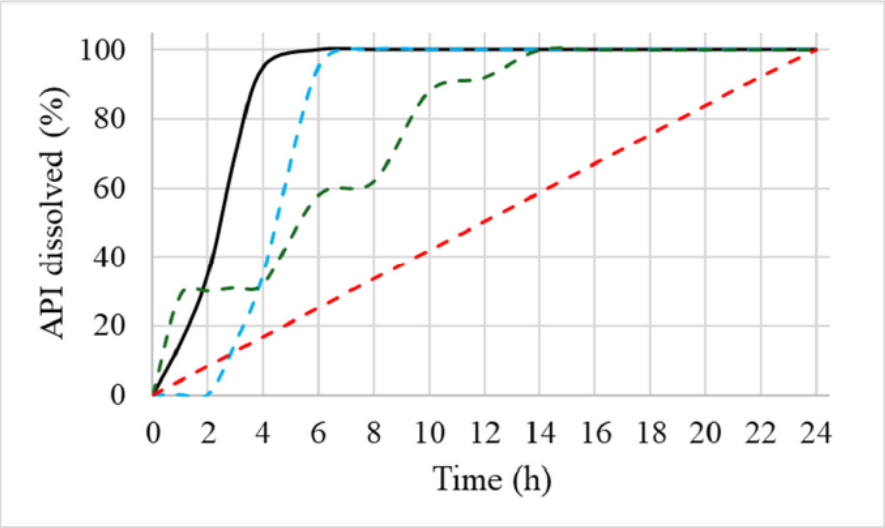

Figure 3: *Release types of the active substance (black: IR, blue: delayed release, green: pulsatile release, red: extended release (zero-order kinetics))*

1.2.2. The osmosis

Osmosis is a restricted diffusion, where particles of solvent migrate across the membrane between solutions of different concentrations on the two sides of the semipermeable membrane. The particle sizes of the solvents are relatively high; thus, these particles are not able to penetrate the membrane. The driving force of osmosis is the pursuit of a concentration balance between the two different solutions. The solvent from the lower concentration solution will diffuse to the higher concentration solution, which will result in a dynamic equilibrium state between the two sides of the semipermeable membrane. In this equilibrium state, the same amount of solvent particles diffuses into the higher concentration solvent, which is squeezed out by the pressure difference. The pressure difference associated with this equilibrium state is called osmotic pressure [31, 32]

1.2.3. History of osmotic pumps.

The effect of osmosis was first studied in 1748, and in 1877, Pfeffer was the first who carried out a quantitative measurement regarding osmosis and osmotic pressure. Since then, the applicability of osmosis in the field of drug delivery has gained more attention [33].

The Rose-Nelson pump:

The first system which used osmosis as the driving force of a controlled active substance delivery mechanism was the Rose-Nelson pump, that was reported in 1955. This pump consisted of three chambers: a drug chamber, a salt chamber and a water chamber. After the administration of the drug delivery system, the water has penetrated the salt chamber through the semipermeable membrane, which separates the two parts. The water penetration increased the volume of the middle chamber (salt chamber), causing the API to be released [34].

The Higuchi-Leeper pump:

In 1970, Alza Corporation was presented a simplified version of the Rose-Nelson pump called the Higuchi-Leeper pump. This system contained only two chambers, a drug chamber and a salt-containing chamber. The water penetrated through a semipermeable membrane from the surrounding environment, which resulted in the release of the active substance [35].

The Higuchi-Theeuwes pump:

Like the Higuchi-Leeper pump, the Higuchi-Theeuwes pump also contained salt and API containing chambers. In this case, the drug chamber was placed as the core of the delivery system, and the salt chamber, which was a dispersion in a suitable carrier, was placed surrounding the API core. The active substance was released through a drug delivery orifice designed on the pump [36].

Elementary Osmotic Pump (EOP):

A further step towards the intensive application of the osmotic drug delivery system was the EOP. The EOP is a compressed monolayer tablet which contains the API with excipients. The tablet is coated with a semipermeable membrane. The membrane is provided with a hole that acts as the drug delivery orifice. In the case of the formulation

of the EOP, active substances with good water solubility are used [37]. Several EOP was approved and marketed in the recent years, such as Acutrim, Efidac 24, Minipress XL, Volmex, Sudafed 24, Teczem and Altoprev® [38].

1.2.4 The push-pull type tablets

The structure and mechanism of action of the bilayer osmotic tablets:

In the instance of a conventional bilayer tablet, one of the layers contains the osmogene excipient with a high amount of swellable polymer. The other layer contains the API. The tablet is coated with a semipermeable coating, which allows only water and small molecules to penetrate through and denies the API from being liberated uncontrolled from the whole surface of the tablet. The controlled active substance liberation is provided by the osmosis process. The presence of the osmogene in the so-called “push layer” creates an osmotic pressure difference between the two sides of the semipermeable membrane. The water diffusion into the osmotic core causes the polymers to swell on contact with water. The volume increase of the push layer will push out the API from the so-called “pull layer” through a drug delivery orifice designed on the coating of the tablet. The external layer of these osmotic drug delivery systems is usually a coloured coating which contains red iron-oxide or titanium-dioxide, or other natural or artificial colouring agents. This coating hides the bilayer tablet and the semipermeable coating before the intake of the medicine [39, 40]. The structure and mechanism of action of a conventional bilayer tablet are shown in Figure 4.

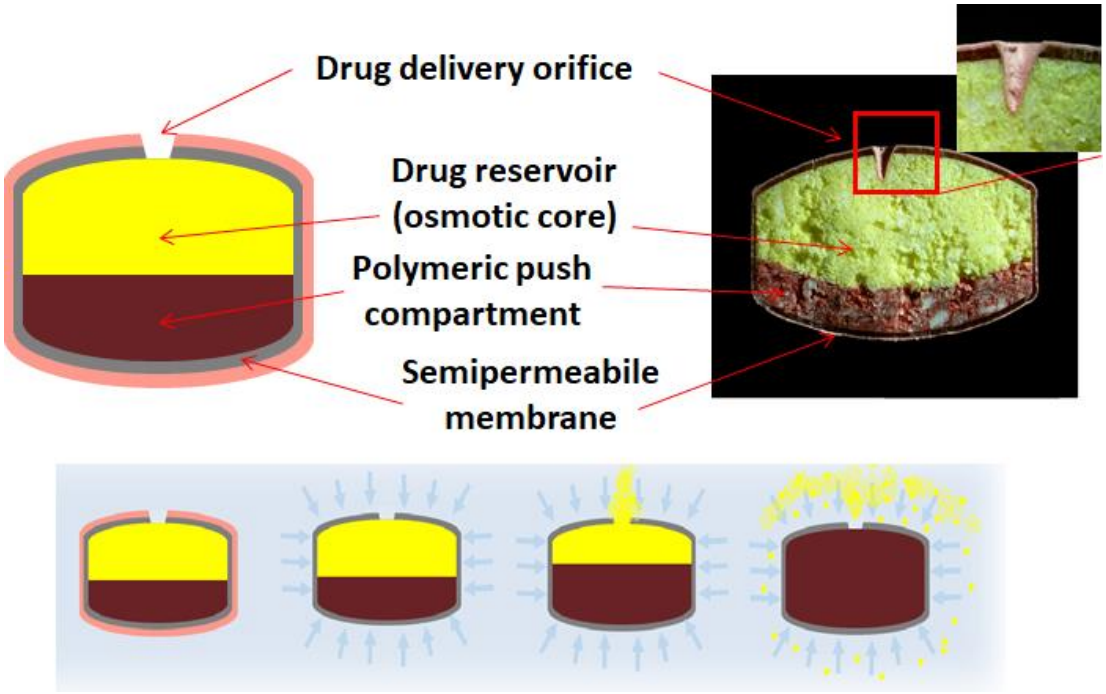

Figure 4: *The structure and mechanism of action of the bilayer osmotic drug delivery system*

The structure and mechanism of action of the trilayer osmotic tablets:

The drug delivery mechanism and the driving force of the liberation of the active substance correspond to the conventional bilayer OROS tablets; the main difference between them lies in their structure. The osmotic delivery systems with three chambers contain one layer with osmogene and swellable polymer excipients, and two API containing layers, which are placed either in the middle and the top, or at the top and the bottom of the tablets. If the active substance is in both the bottom and the top layer, these tablets are called sandwich tablets. The API is released from the osmotic delivery system through well placed drug delivery orifices, that is drilled into the semipermeable coating. Invega extended-release formulation is an example of a marketed trilayer osmotic tablet [41, 42]. A picture of the Invega extended-release tablet is shown in Figure 5.

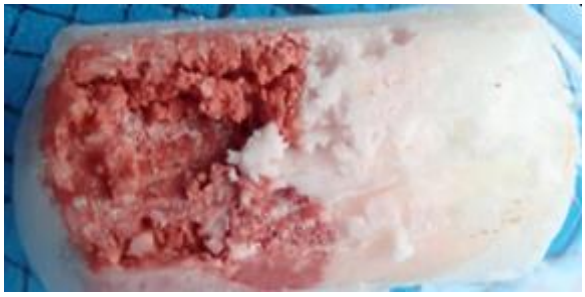

Figure 5: *Swelling mechanism demonstrated by not allowed halving of the bilayer osmotic tablet (cross sectional view)*

In case of every osmotic drug delivery system, an important limitation is that the patient must swallow these tablets, since the structural integrity of these tablets is necessary to achieve the controlled and prolonged release; thus, the patients cannot chew or crush the tablets. Crushing of the tablets can lead to altered drug release and toxicity as well [43].

1.2.5. The formulation of osmotic drug delivery systems

The formulation of oral osmotic drug delivery systems contains multiple steps. The osmotic core, which usually consists of one, two or three layers compressed together with compression machines. The cores are coated with semipermeable membranes. A drug delivery orifice must be drilled to the surface of the tablet either by mechanical drill or with a laser beam [44]. In the instance of a controlled porosity osmotic pump, pore-forming agents are used in the semipermeable coating. These materials dissolve on contact with the liquids and in situ form the drug delivery orifices [45]. Modified punches can also be used to formulate a drug delivery orifice. With the modified punches, the drug delivery orifice is pierced under the compression force [46]. The optimal size of drug delivery orifices in the case of osmotic delivery systems is between 600 μm and 1 mm [44].

1.2.6 Advantages and disadvantages of OROS

The osmotic drug delivery systems have several advantages. These systems have a zero-order drug release kinetics, so they can ensure more consistent blood levels compared to conventional, IR tablets. In addition, osmotic tablets have fewer side effects. Their drug release is controlled by their specific composition and structure, which ensures the prolonged API release. The release of the active substance is independent of the pH and the gastrointestinal motility; thus, the patient can take the medicine, so the

administration time is independent of the effect. Moreover, these formulations have a more favourable dosing regimen (once a day); therefore, the patient compliance can be increased [47, 48]

It is important to acknowledge some limitations in the case of OROS tablets. Due to their special structure, complicated manufacturing is required, which leads to high production costs. Osmotic drug delivery systems have to be taken without crushing or chewing the tablets [49]. Osmotic tablets can cause gastrointestinal occlusion, and if an irritative API was selected during formulation, it can cause gut wall irritation as well [50]. Further disadvantage of the osmotic drug delivery systems, that the damage or defective coating can cause dose dumping [51].

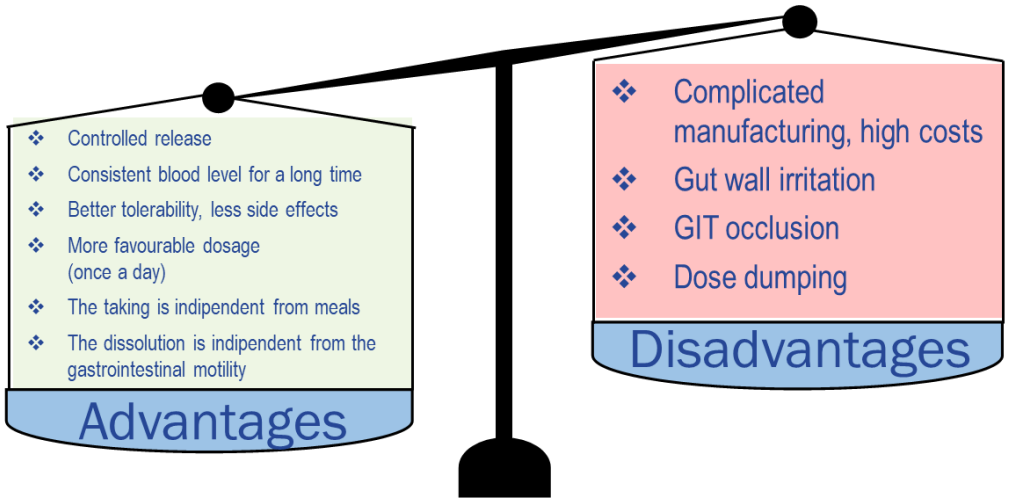

Figure 6: *Advantages and disadvantages of osmotic drug delivery systems*

1.3. The importance of particle size in pharmaceutical technology

The particle size of both drugs and excipients plays a key role in ensuring the sufficient physical properties of the dosage form, and the programmed and controlled release of the active substances [52]. To ensure the ideal particle size, 3D printed milling bodies provide a promising, flexible possibility for the pharmaceutical industry.

1.3.1 Particle size reductive methods

Although wet milling is required in micronization of the materials, dry milling remains a well-established method for preprocessing in the instance of raw materials. Numerous methods can be applied in the case of dry media milling to reduce the particle size of pharmaceutical materials, such as hammer milling, jet milling, roller milling and ball milling [53-55]. Milling balls are produced from a variety of hard materials, such as

steel grinding media and cast iron [56], cemented tungsten carbide [57], agate-, glass-, and zirconia-based media [58]. Guner et al was used polystyrene grinding balls and compared their warming up and breakage kinetics with conventional zirconia milling bodies during wet bed milling [59].

1.3.2. The influencing parameters of ball milling on particle size distribution

Particle size and particle size distribution can be adjusted and influenced by many factors and parameters during the ball milling process. The quantity and the size of the grinding balls influence the particle size distribution of the ground materials. By increasing the quantity and decreasing the size of the milling bodies, the particle size of the comminuted materials is decreased [60, 61]. During industrial milling procedures, a mixture of different-sized milling balls is usually applied, since with the mixture of different grinding balls, a more efficient milling can be performed [62]. With the increase in the milling time, the particle size of the powder is decreased, although by increasing the time, there is a limitation in the maximum particle size that can be achieved by applying further milling time, the final particle size will remain unchanged [63, 64]. Rotation speed is also considered a crucial milling parameter from the point of particle size reduction. The higher the milling speed is, the bigger the milling rate is in ball milling procedures [65]. According to the rotation speed, two factors have to be taken into consideration. The maximum effective rotation speed is called the critical speed. Above this revolution rate, the balls are positioned stationary relative to the inner surface of the grinding jar, preventing them from engaging in the grinding process; thus, the comminution rate must be set below the critical speed [66]. Another limiting factor of the rotation speed is the temperature of the system. During the milling, the grinding balls collide with each other and with the wall of the grinding jar, and an excessive amount of heat is generated as a result of these collisions [67]. The heat generation of the temperature can cause the degradation of the heat-sensitive materials [68]. Moreover, the elevation of the temperature in the system during ball milling can also result in the amorphization of certain materials, which can lead to thermodynamically unstable products [69]. In wet milling, achieving a smaller final particle size is facilitated by effective simultaneous cooling, whereas heat generation during dry milling presents a significant challenge [68, 70].

2. Objectives

The aim of the current research was to utilize 3D printing as an emerging and flexible tool of the pharmaceutical technology in the design and fabrication of a push-pull type osmotic drug delivery system, which enables the controlled release of the drug, that is fitted to the individual needs of the patients. The concept was that the complex structure of the drug delivery system was assembled from elements akin to Lego® blocks to be able to tailor the drug delivery and achieve personalized medication. The optimal push and pull layers, semipermeable membrane and the 3D printed skeleton of the OROS must be constructed to enable this innovative formulation to achieve the zero-order kinetic release profile of the active substance, which is independent of the gastrointestinal motility, that was targeted in the research.

The particle size of the APIs and the excipients plays a crucial role in the performance of the delivery systems. Another objective of the research was to investigate the potential applicability of using AM in dry media ball milling as a particle size reductive method to replace conventional milling media materials with more flexible resins. Because one of the advantages of the chosen SLA printing method is that an extensive heat transfer can be avoided, it was aimed to avoid the warmup of the system during grinding with the application of additively manufactured dry media milling balls. The comparative evaluation focused on the temperature elevation of stainless-steel balls and their replacement with 3D printed photopolymer resin grinding media in the traditional dry ball milling process, serving as a model for those cases where conventional materials cannot be used in milling.

3. Methods

3.1. Preparation of the elements of the osmotic delivery system

3.1.1. Compression of the layers of the complex formulation

In the instance of the pull layer, the quinine hydrochloride model active substance (obtained from: Magilab Kft., Budapest, Hungary), the Pharmacoat 606 HPMC (obtained from: Shin-Etsu Chemical Co. Ltd., Tokyo, Japan) and the magnesium stearate (obtained from: Molar Chemicals Ltd., Halásztelek, Hungary) were mixed at 40 rpm for 20 minutes in a V-blender (Xinxiang Chenwei Machinery Co., Ltd., Xinxiang, China). The batch size was 200 g. The composition of the pull layer is shown in Table I.

In the case of the push layer, Metolose 90-SH 4000 SR (obtained from: Shin-Etsu Chemical Co. Ltd., Tokyo, Japan), sodium chloride (obtained from: Molar Chemicals Ltd., Halásztelek, Hungary), iron (III) oxide (obtained from: Fisher Scientific UK, Loughborough, United Kingdom), talc (obtained from: Molar Chemicals Ltd., Halásztelek, Hungary) and magnesium stearate (obtained from: Molar Chemicals Ltd., Halásztelek, Hungary) were homogenised with the parameters given above. The batch size was 200 g. The composition of the push layer is shown in Table II.

Table I: The composition of the pull layer

Name of the material	Material quantity (w/w%)	Role in the composition
Quinine hydrochloride	25.0	API
Pharmacoat 606 HPMC	74.5	swelling polymer
Magnesium stearate	0.5	lubricant

Table II: The composition of the push layer

Name of the material	Material quantity (w/w%)	Role in the composition
Metolose 90-SH 4000	72.5	swelling polymer
Sodium chloride	25.0	osmogene
Iron (III) oxide	1.0	colouring agent
Talc	1.0	glidant
Magnesium stearate	0.5	lubricant

The push and pull layers of the osmotic drug delivery system were compressed separately with the Fette Exacta 1 (Fette Compacting GmbH, Schwarzenbek, Germany) single-punch compression machine. The compression speed was 40 tablets/minute, round shaped punches with a diameter of 14 mm were applied in the compression. The weight of each individual tablet was 400 mg each.

3.1.2. Preparation of semipermeable film

The cellulose acetate (CA) polymer (Mn~30000, weight: 9.45 g, obtained from: Merck KGaA, Darmstadt, Germany) with plasticizers dissolved in acetone (weight: 131.1 g, obtained from: Molar Chemicals Ltd., Halásztelek, Hungary) on a magnetic stirrer. The stirring speed was 50 rpm. The plasticisers were propylene glycol (PG) (obtained from: Hungaropharma Zrt., Budapest, Hungary) alone or propylene glycol with glycerol (GLY) (obtained from: Molar Chemicals Ltd., Halásztelek, Hungary).

The semipermeable membrane from the prepared coating solutions was formulated with vertical layering, spraying and film casting methods (shown in Figure 7). From these methods, only the film casting was a suitable method to prepare films that met the needs of the innovative delivery system. From the different coating solutions, films with different thicknesses (50/ 100/150/200/250 μm) were cast with an Elcometer 3580 Casting Knife Applicator (Elcometer Limited, Manchester, United Kingdom). Four different types of semipermeable films were cast depending on the plasticizers and the preparation temperatures in different thicknesses. The cast films are shown in Table III.

Table III: The casted films

The marking of the film	**The plasticizer(s)**	**The ratio of plasticizers and CA (w:w)**	**Preparation temperatures (°C)**
A-25	PG	CA:PG= 1:1	25 ± 2
A-40	PG	CA:PG= 1:1	40 ± 2
B-25	PG, GLY	CA:PG:GLY= 1:1:1	25 ± 2
B-40	PG, GLY	CA:PG:GLY= 1:1:1	40 ± 2

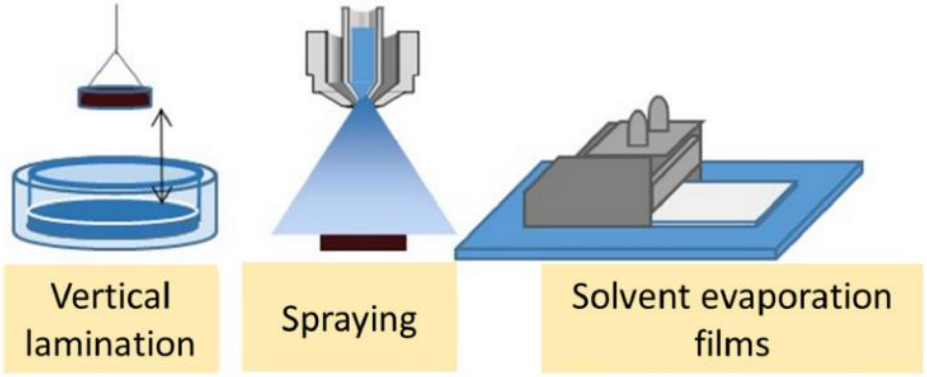

Figure 7: *Tested film preparation methods*

The cast films were placed in the drying chamber for 24 hours to allow the solvent to fully evaporate. The dried films were peeled off the surface and stored in aluminium foil for further analysis.

3.1.3. Design and fabrication of the additively manufactured frame

The 3D objects were designed with Autodesk Fusion 360 (Autodesk Inc., San Rafael, CA, USA). The planned object contained a thread between the upper and bottom parts, which ensures that the two layers and the semipermeable membrane can be inserted easily into the frame, and the frame can be closed before the examinations. The length of the thread was 4.0 mm, the size was 17.0 mm, and it was designed as 17x1.5, and the direction was right-handed. The size and shape of the 3D frame were designed according to the size and geometry of the layers. Because of the flexibility and easy modification of the designs used for AM, with any modifications on the push or pull layers to achieve the goals of personalized medications, the 3D printed frame can be modified easily. The diameter of the bottom part of the frame was 16.85 mm, and the thickness was 5.4 mm. Into the centre of this part, a hole with a diameter of 14.5 mm was planned to secure the space for the insertion of the push, the pull and the semipermeable membrane. The upper part of the frame was designed with a diameter of 18.5 mm and with four drug delivery orifices on the top of the frame. The diameter of the orifices was 2 mm each. The images of the CAD file are shown in Figure 8.

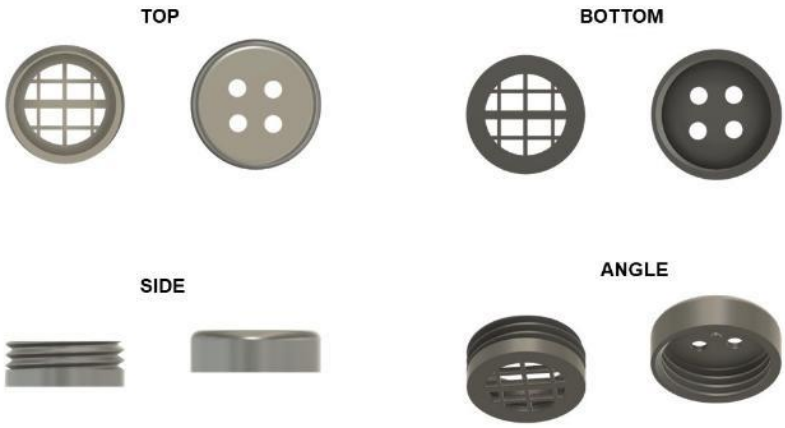

Figure 8: *The CAD file of the frame from different views [11]*

The stereolithography file of the planned object was sliced in the Prusa Slicer (Prusa Research a.s., Prague, Czech Republic) slicing software. The slicer divides the object into several, well-defined horizontal slices. The set parameters during the slicing were the following: layer thickness was 0.025 mm, the initial exposure time was 10 seconds, and the exposure time was 2 seconds. No supports were planned below the objects.

The SL1S file obtained from the slicing was transported to the Original Prusa SL1S Speed 3D printer (Prusa Research a.s., Prague, Czech Republic). The printer was an SLA type printer, and Raydent Crown & Bridge Resin (obtained from Zortrax S.A., Olsztyn, Poland) was used to print out the 3D frame. The printlets were cleaned and postcured in the Original Prusa Curing and Washing Machine (Prusa Research a.s., Prague, Czech Republic). The printlets were cleaned for 5 minutes in isopropyl alcohol (obtained from: Molar Chemicals Ltd., Halásztelek, Hungary). The cleaned printlets were dried and UV postcured for 3-3 minutes.

3.2. Examinations of the complex osmotic drug delivery system

3.2.1. Physical characterization of tablets

The weight uniformity test was performed with 20 pieces of tablets with Kern ANJ-NM/ABS-N analytical balance (Kern&Sohn GmbH, Balingen, Germany), the standard deviation (SD) was calculated from these data. Erweka TBH 200 TD (Erweka GmbH, Langen, Germany) was used to measure the hardness, the height and the diameter

of the push and pull tablets for 10 tablets and the SD was calculated from these data. The friability test was performed in the Erweka AR apparatus (Erweka GmbH, Langen, Germany). All measurements were conducted in accordance with the specifications outlined in European Pharmacopoeia (Ph. Eur.) 11.

3.2.2. Physico-chemical characterization of cast films

Contact angle measurements:

10 µl of distilled water was dropped on the polymer films from above at a distance of 10 mm. The thickness of the polymer film was 100 µm. Pictures from the membrane with the distilled water droplet were taken with Keyence VHX-980 Lens Z20 (Keyence International, Osaka, Japan) every 20 seconds. For the purpose of better visibility, 1% methylene blue was added to the distilled water. The magnification was 50x, the lens and the camera were tilted at an angle of 90°. The analysis of the photos was carried out using Fifi Image J Software Contact Angle Plug-In (Image J NIH, USA) to determine the contact angles for each membrane.

Mechanical properties of films:

The film strength (FS) of dry films was measured with a Brookfield CT3-4500 Texture Analyser (Brookfield Eng. Lab. Inc., USA) operating with a 4.5 kg load cell. TA-18 stainless steel spherical probe (30 g; diameter: 12.7 mm) was employed in rupture mode with a specific target load. The probe descended at a speed of 0.5 mm/s, while the load was recorded as a function of the film elongation. The membranes (thickness: 100/150/200/250 µm) were fixed in Brookfield TA-RT-KIT with TA-FSF (film support fixture) (d=20 mm). Brookfield Texture ProCT software (v1.4 Build 17) was used to create the report about the elongation of the film in the percentage deformation of the films. Each batch was analyzed in triplicate.

Positron Annihilation Lifetime Spectroscopy (PALS):

The positron source used for PALS measurements consisted of carrier-free ^{22}NaCL sealed between thin (2 mgcm^{-2}) Kapton foils. The source had an activity of approximately 5.10^{-5} Bq. PALS measurements were conducted using a fast-fast coincidence setup equipped with two BaF_2 crystal detectors. The photomultiplier tubes were Philips XP 2020Q models (Koninklije Philips N.V., Eindhoven, Netherlands) and the measurement electronics were assembled from standard ORTEC components. About

230 ps was the time resolution of the system. Positrons' lifetime varies with the surrounding electron density. Positrons are also utilized to scan the momentum distribution of electrons within the materials. The energy of the resulting annihilation photons reflects the momentum of the annihilated electrons, causing a broadening of the gamma-ray line [71].

A germanium gamma detector was used to record the Doppler-broadening spectra. The resolution was 1.1 keV for the annihilation photopeak. The spectra were evaluated based on the S-parameter, which indicates the width of the annihilation photopeak. Generally, higher S-parameter corresponds to lower momentum in annihilating electrons. Each batch was examined in triplicate.

Water content determination of membranes:

Metrohm 787KF Titrino Karl-Fischer titrator (Metrohm AG, Herisau, Switzerland) was used for the measurement of the water content of the different membranes. During the titration, Polytron PT 1600 E (Kinematica AG, Malters, Switzerland) was used for mixing. Before the measurements with the membrane samples, the water equivalency factor of Aquastar® CombiTitrant-5 (obtained from: Merck & Co., Rahway, NJ, USA), Karl-Fischer reagent was established by titrating 10 µl of MiliQ water. The solvent during the titration was extra dry methanol (obtained from: Merck & Co., Rahway, NJ, USA) was titrated with the reagent before the measurements of the membrane samples. In the instance of each batch, 5 membranes were analyzed, and the SDs were calculated from the measured data.

Scanning electron microscopic (SEM) images of membranes:

The SEM images of the membranes were captured with Jeol JSPM-5200 Scanning Probe Microscope (Jeol Ltd., Tokyo, Japan with 15 kV voltage with gold coating during the sample preparation procedure.

Permeability test of different membrane samples:

The permeability of different membranes was tested with the Franz Vertical Diffusion Cell (Hanson Research, Los Angeles, CA, USA). The temperature of the diffusion cell during the tests was 37°C, and the acceptor medium was distilled water. In the instance of the salt permeability study, 100 mg sodium chloride was placed on the top of the membrane inserted into the Franz cell, and at each sampling point, a 60 µl sample

was taken and analysed with Gonotech Osmomat 030 (Gonotec GmbH, Berlin, Germany). The sampling times were: 5 min, 15 min, 30 min, 45 min, 1 h, 2 h, 3 h, 4 h. Each batch was analyzed in triplicate. In case of pH permeability tests, the Franz diffusion cell was tempered to 37°C, and water for injection was used as the acceptor medium. A buffer with pH 1.2 was measured on the top of the membrane. The volume of the buffer that was used was 4 ml. A 0.5 ml sample was taken at every sampling time and analysed with a Mettler-Toledo Seven Compact micro pH/Ion meter (Mettler-Toledo International Inc., Columbus, OH, USA). The sampling times were the same as those used for the salt permeability test. Each batch was analyzed in triplicate.

3.2.3. Investigation of osmotic release drug delivery system

In vitro dissolution study:

Dissolution tests were carried out with the USP dissolution apparatus II (paddle method; Hanson Reseach, USA). The system was tempered to 37.0 ± 0.5°C. The volume of the dissolution medium was 900 ml in each vessel. The pH of the dissolution medium was pH 1.2 hydrochloric acid in the first hour, and pH 6.8 between 1 and 24 hours. The in vitro dissolution tests of the different tablets were carried out in a spiral copper sinker (length: 37 cm; diameter: 0.6 mm; mass: 1g). 5 ml filtered samples (10 μm; Hanson Research, USA) were withdrawn automatically from the vessels. In every sampling point, the withdrawn media was replaced. Concentrations were determined from the measured absorbance values. The absorbance of the samples was measured with an Agilent 8453 spectrophotometer (Agilent Technologies Inc., Santa Monica, CA, USA) at 346 nm for samples collected within the first hour and at 318 nm for samples withdrawn between 1 and 24 hours. Each batch was analyzed in triplicate. The obtained release profiles were analyzed with zero-, first-order kinetics as well as Higuchi and Korsmeyer-Peppas models.

Digital microscopic images of the drug delivery system:

Digital microscopic images from the osmotic release drug delivery system were captured with a Keyence VHX 970 Digital Light Microscope (Keyence International, Osaka, Japan).

3.3. Application of 3D printing in dry media ball milling

3.3.1 Design and fabrication of grinding balls

The models of the grinding balls were designed with Autodesk Fusion 360 (Autodesk Inc., San Rafael, CA, USA) in different sizes (d: 25 mm, d: 20 mm, d: 10 mm). The designs of the objects were sliced in Prusa Slicer (Prusa Research a.s., Prague, Czech Republic) slicer program, and the obtained SL1S files were transported into an SLA type 3D printer. The printlets were printed with the Original Prusa SL1S Speed 3D printer (Prusa Research a.s., Prague, Czech Republic). The resin for the printing was Prusament Resin Tough Prusa Orange (obtained from: Prusa Research a.s., Prague, Czech Republic). The layer thickness in the AM was 0.025 mm in each layer, with supports below the printlets. The initial exposure time was 25 seconds in the first three layers, and the exposure time was 6 seconds for the further layers. The printlets were cleaned with isopropyl alcohol (obtained from: Molar Chemicals Ltd., Halásztelek, Hungary), and dried, UV postcured for 3-3 minutes in the Original Prusa Curing and Washing Machine (Prusa Research a.s., Prague, Czech Republic).

3.3.2. Examinations with the 3D printed grinding media balls

Microscopic images:

Digital microscopic pictures from the grinding balls and the initial and ground saccharose were captured with Keyence VHX 970 Digital Light Microscope (Keyence International, Osaka, Japan)

Densities of the different milling balls:

The mass of the different grinding balls was measured with a Kern ABJ-NM/ABS-N analytical balance (Kern & Sohn GmbH, Balingen, Germany). The densities of the 3D printed and the comparator stainless steel milling balls were calculated.

Weight loss test of the milling balls:

Weight loss test of the different-sized additively manufactured milling balls was performed in the Retsch 100 PM (Retsch GmbH, Haan, Germany) planetary ball mill, the weight of the grinding bodies was measured before and after the process with Kern ABJ-NM/ABS-N (Kern & Sohn GmbH, Balingen, Germany). The initial weight of the samples

was 40 g in each measurement. The process time was 15 min at 300 rpm with a 5 min break time and a 5 min interval time. The total revolutions were 3000.

Grinding studies with saccharose model material:

For the comminution of the saccharose model material (obtained from: Molar Chemicals Ltd., Halásztelek, Hungary), the Retsch PM100 (Retsch GmbH, Haan, Germany) planetary ball mill was used, the milling rate was 200 rpm, the total procedure time was 15 min with a 5 min break time and a 5 min interval time. The measurements were performed with 3D printed balls in different sizes and quantities. As a comparator grinding medium, conventional stainless steel milling balls (Retsch GmbH, Haan, Germany) were used with the same diameters as the 3D printed balls. The initial and ground particle size of the saccharose was measured with Retsch AS 200 (Retsch GmbH, Haan, Germany) control vibrational sieve with the amplitude of 1.5 mm. The sieving time was 5 minutes. Each procedure was measured under the same conditions in triplicate.

Structural changes of lactose monohydrate during the milling process:

The grinding of the lactose monohydrate (obtained from: Molar Chemiclas Ltd., Halásztelek, Hungary) was performed in a planetary ball mill. The revolution speed was 400 rpm, and the milling time was 45 minutes. During the procedure, an equal quantity of grinding media with identical diameters was used from both the printed model grinding bodies and the comparator stainless steel balls. The diameters and quantities of the grinding bodies (additively manufactured and stainless steel) during the operation were the following: d= 25 mm (1 piece), d= 20 mm (5 pieces) and d= 10 mm (3 pieces). After 45 minutes of milling, the ground lactose samples were measured with a Seiko Exstar 6000/6200 (Seiko Instrument Inc., Chiba, Japan) differential scanning calorimeter (DSC). A dispensed amount of 8 mg lactose monohydrate was placed into aluminium pans and analysed at a 10 °C/ min heating rate from 0 °C to 200 °C.

Warming of the grinding jar and the milling balls:

The warming of the system was monitored by thermal imaging technique with a Voltcraft WBS-220 (Conrad Electronic International GmbH & Co. KG., Hirschau, Germany) thermal camera. The warming is caused by the friction between the milling balls and the grinding jar. The details of the milling balls, used in the warmup tests were the following: d= 25 mm (1 piece), d= 20 mm (5 pieces) in the case of both the 3D printed

and the conventional stainless-steel balls. Pictures with the thermal camera were captured after 45 minutes of the milling process from the same position in every procedure. The milling rate was 400 rpm. The thermal camera was focused automatically on the warmest point of the system. The temperature of the warmest point was used for further analyses. The setup of the measurement is shown in Figure 9.

Figure 9: *Warmup measurement setup [72]*

4. Results

4.1. The modular, osmotic release drug delivery system

4.1.1. Physical characterization of the tablets

The in-process control measurements with both the push and pull tablets were conducted in accordance with the Ph. Eur., and the results verified that both tablets complied with the standards set by the Pharmacopoeia. The results of the investigations carried out in the two layers are shown in Table IV.

Table IV: Results of the in-process control measurements

	mass (mg)	**height (mm)**	**diameter (mm)**	**hardness (N)**	**friability (%)**
Pharmacopeial requirements	RSD > 5%	-	-	> 25N	< 1%
push layer (SD)	395.3 (± 5.06)	2.20 (± 0.03)	14.1 (± 0.01)	30.4 (± 4.25)	0.21
pull layer (SD)	405.6 (± 0.00)	2.96 (± 0.01)	14.1 (± 0.01)	33.3 (± 2.20)	0.81

4.1.2. Macro- and microstructural characterization of membranes

The wetting characteristics of the different membranes are shown in Figure 10. The contact angle measurements showed that the glycerol containing membranes have improved wetting with lower contact angles. Furthermore, the membranes cast at 40°C had enhanced wettability compared to membranes prepared at 25 °C.

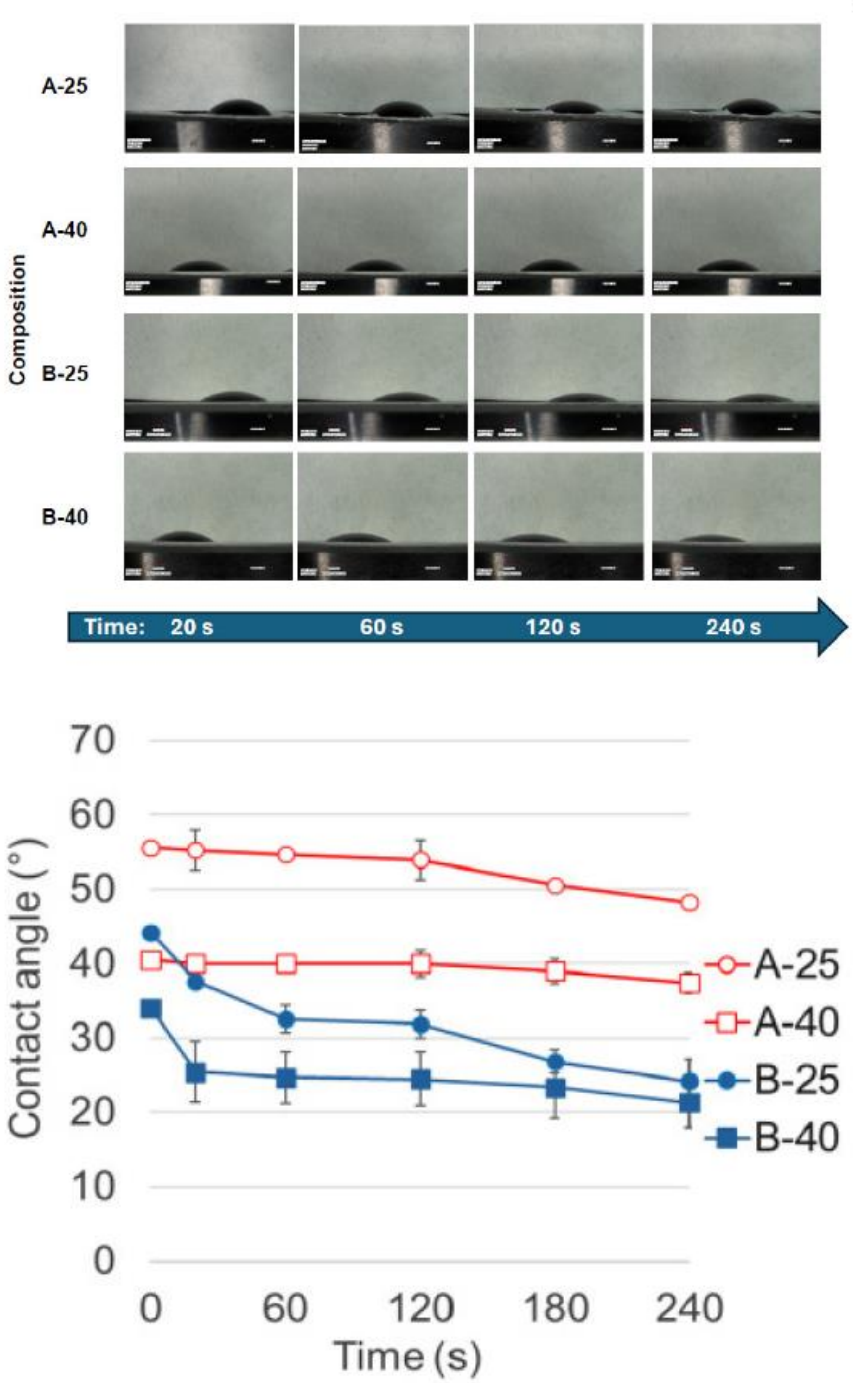

Figure 10: *Contact angle determination of the different membrane compositions [11]*

The results of the contact angle measurements were supported by the results of the PALS measurements. The o-Ps lifetime values, which describe the free volume characteristics of the sample, were proved that the glycerol containing membranes have smaller-sized, but an increased number of holes in their structure compared to the membranes contained only propylene glycol. In the instance of membrane A-25, the

increase in the size of the holes was thickness dependent. Significantly larger o-PS values were measured in the case of B-40 membrane, which correspondent to free volume holes. The elevation in the casting temperature of the membranes resulted in a more relaxed, mobile structure, with higher chain mobility.

The o-Ps lifetime measurements align well with the S- and W-parameter measurements of the PALS, which reflect the chemical structure at the annihilation site. The general evaluation of the S- and W-parameters is shown in Table V. The secondary bonding between components can be identified based on the evaluation of these parameters of the PALS measurements. The glycerol containing membrane compositions (B-25 and B-40) have H-bridges in their structures according to the S- and W-parameters of these membranes

Table V: Evaluation of S- and W-parameter

	S parameter	**W parameter**
High number of low kinetic energy e^- pairs	large	small
Bonded electrons	small	large

Based on the Doppler-broadening spectra, the positrons in the membranes plasticized by propylene glycol and glycerol interacted with a greater number of electrons possessing higher momentum, which corresponds to the reduced hole size. The results of the PALS measurements are shown in Figure 11. The glycerol within the membrane serves to separate polymer chains, weakening the intermolecular forces between adjacent chains and lowering brittleness, which improves the films' flexibility and stretchability [73].

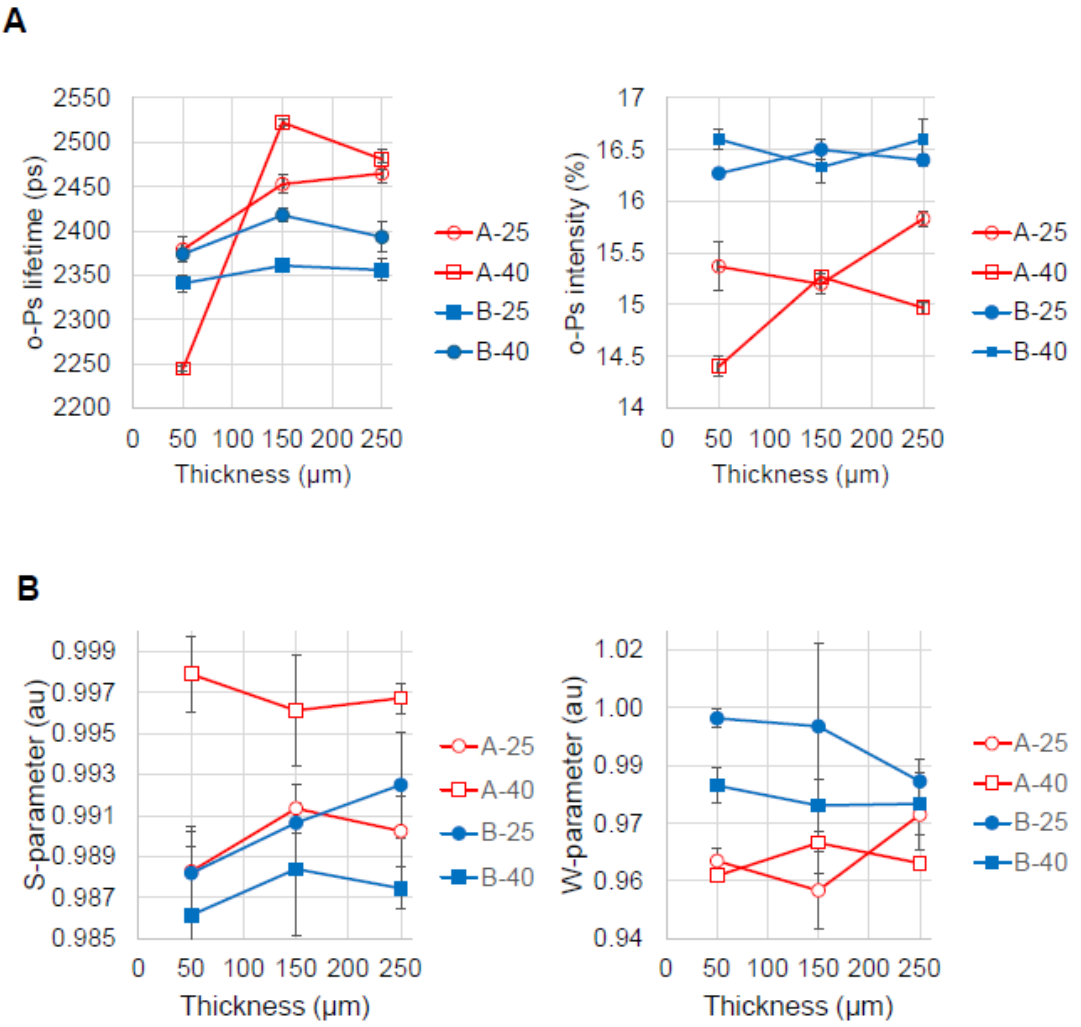

Figure 11: *A: Positron lifetime measurements of the different membrane formulations in different thicknesses B: Doppler broadening spectrum of the different membrane formulations in different thicknesses [11].*

The Karl-Fischer titration of the different membrane formulations was showed that the membranes that contained glycerol as plasticizer had higher water content (B-25 and B-40) compared to those which contained only propylene glycol (A-25 and A-40). The water content of the membranes decreased with the increase in the membrane casting temperature. The results of the water content determinations are shown in Table VI. These findings correspond with PALS results, where the presence of glycerol in the composition led to greater water content due to water occupying free volume spaces.

Table VI: Water content determination for different membranes

Membrane composition	Water content (%)
Comp. A-25	8.12 ± 0.46
Comp. A-40	6.33 ± 1.17
Comp. B-25	11.15 ± 0.55
Comp. B-40	10.04 ± 0.25

The mechanical and morphological examination of the films was performed, and the results have confirmed the plasticizing and pore-forming properties of the glycerol. The Sem microscopic image of membrane composition B-25 is shown in Figure 12.

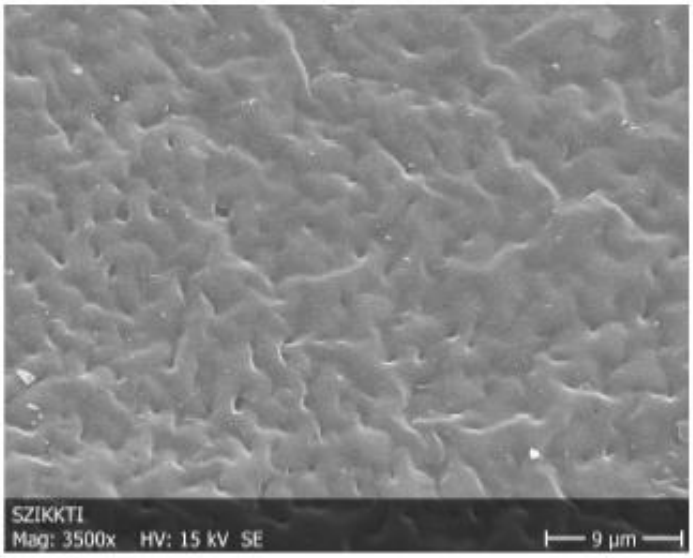

Figure 12: *SEM image of membrane composition B-25 [11].*

Suderman et al were observed that the incorporation of glycerol into the membranes improves the transparency and mechanical properties of the film with increased thickness due to stronger capillary forces that enhance water absorption [74]. The enhanced mechanical properties of the thicker membranes can be attributed to the increased water uptake, driven by their capillary pressure. The elongation of the cellulose acetate is shown in Figure 13.

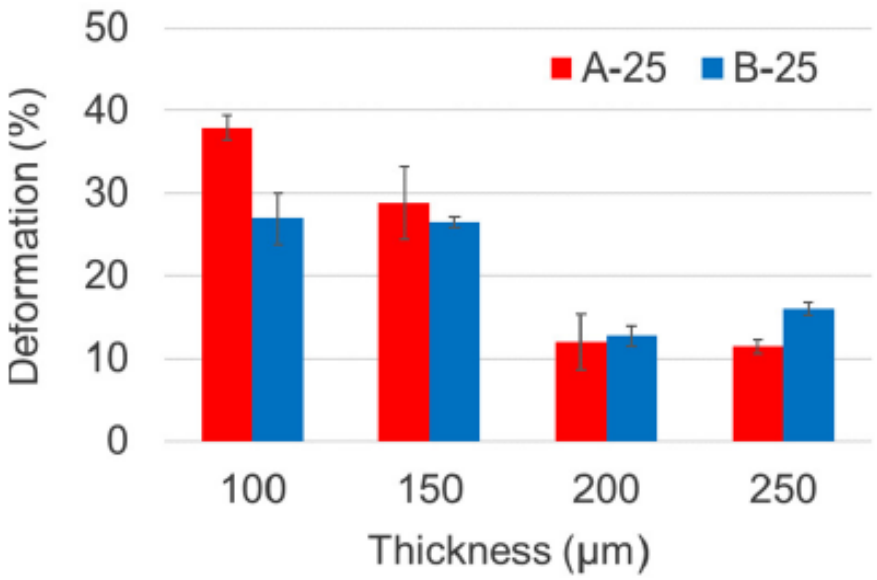

Figure 13: *Elongation of cellulose acetate membranes in different thicknesses [11].*

4.1.3. Membrane permeability measurements

Permeability of sodium chloride through cellulose acetate membranes:

A modified Franz diffusion cell was used to examine the permeability of sodium chloride through different membrane compositions, cast at different temperatures. The results showed that those membrane formulations, which had glycerol plasticizer excipient incorporated into the composition (B-25 and B-40 compositions) had an elevated sodium chloride diffusion. This finding is strongly supported by the PALS measurements and also reflects the pore-forming ability of the glycerol. As a pore former, glycerol dissolves from the membrane on contact with water, which creates pores in the membrane, enabling increased diffusion through the membrane. Figure 14 shows the results of the salt permeability tests.

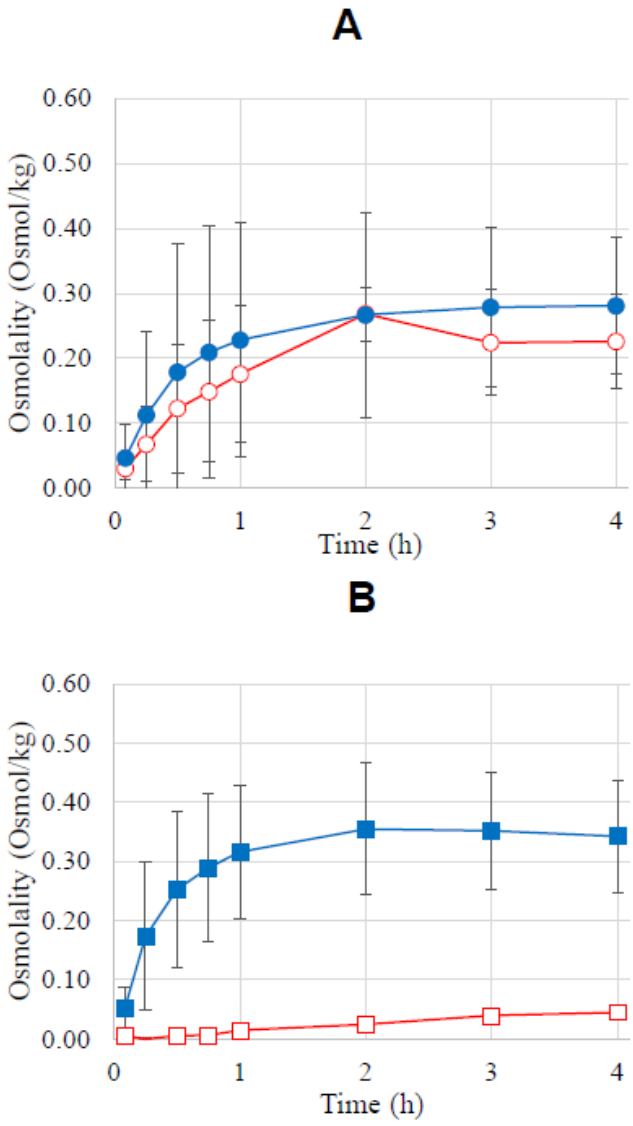

Figure 14: *A: Permeability of sodium chloride through membranes casted at 25°C (thickness: 150 µm, red: A-25, blue: B-25), B: Permeability of sodium chloride through membranes casted at 40°C (thickness: 150 µm, red: A-40, blue: B-40) [11].*

Permeability of pH 1.2 buffer through cellulose acetate membranes:

The diffusion of the pH 1.2 buffer across the membrane was monitored with a Franz vertical diffusion cell. It was experienced that the diffusion of the buffer in the instance of glycerol containing membrane (B-25) was notably faster and more extensive than the membrane that contained only propylene glycol (A-25) as plasticizer.

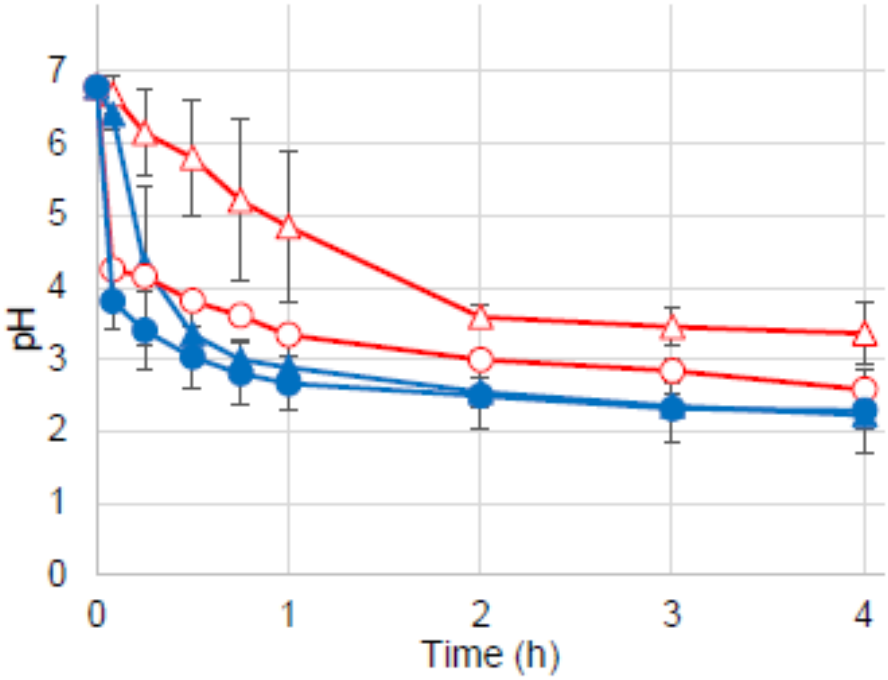

Figure 15: *The permeability of pH= 1.2 buffer across different membranes (red triangle: A-25, 100 µm thickness; red circle: A-25, 150 µm thickness; blue triangle: B-25, 100 µm thickness; blue circle: B-25, 150 µm thickness) [11].*

4.1.4. In vitro dissolution studies

In vitro dissolution studies were performed in the USP dissolution apparatus with the paddle method, with the drug delivery system assembled from different elements. The drug release profiles were depended on the parts that were used (push- and pull layers; the two parts of the 3D printed frame; cellulose acetate semipermeable membranes) to assemble the different structures. The different combinations of the assembled structures are shown in Figures 16 and 17. The obtained drug release profiles were analyzed with zero-order, first-order, Higuchi, and Korsmeyer-Peppas models. The correlation (R) values indicate how well each model fits the data.

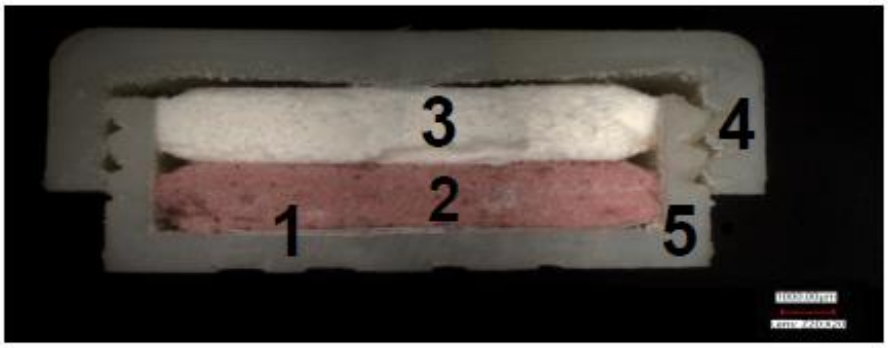

Figure 16: *Cross-sectional digital microscopic picture of the complex osmotic drug delivery system assembled from elements (1: semipermeable membrane; 2: push layer; 3: pull layer; 4: upper part of the 3D printed frame; 5: bottom part of the 3D printed frame) [11].*

In the case of the dissolution tests, the guidelines of the Ph. Eur and the United States Pharmacopoeia (USP) were followed. Based on these guidelines, the pH of the dissolution medium was 1.2 for the first hour and pH 6.8 phosphate buffer was used for the rest of the 24 hours dissolution tests [Ph.Eur 11. 5.17.1.] [75]. The thickness of the membranes that was used in the dissolution tests was 100 μm.

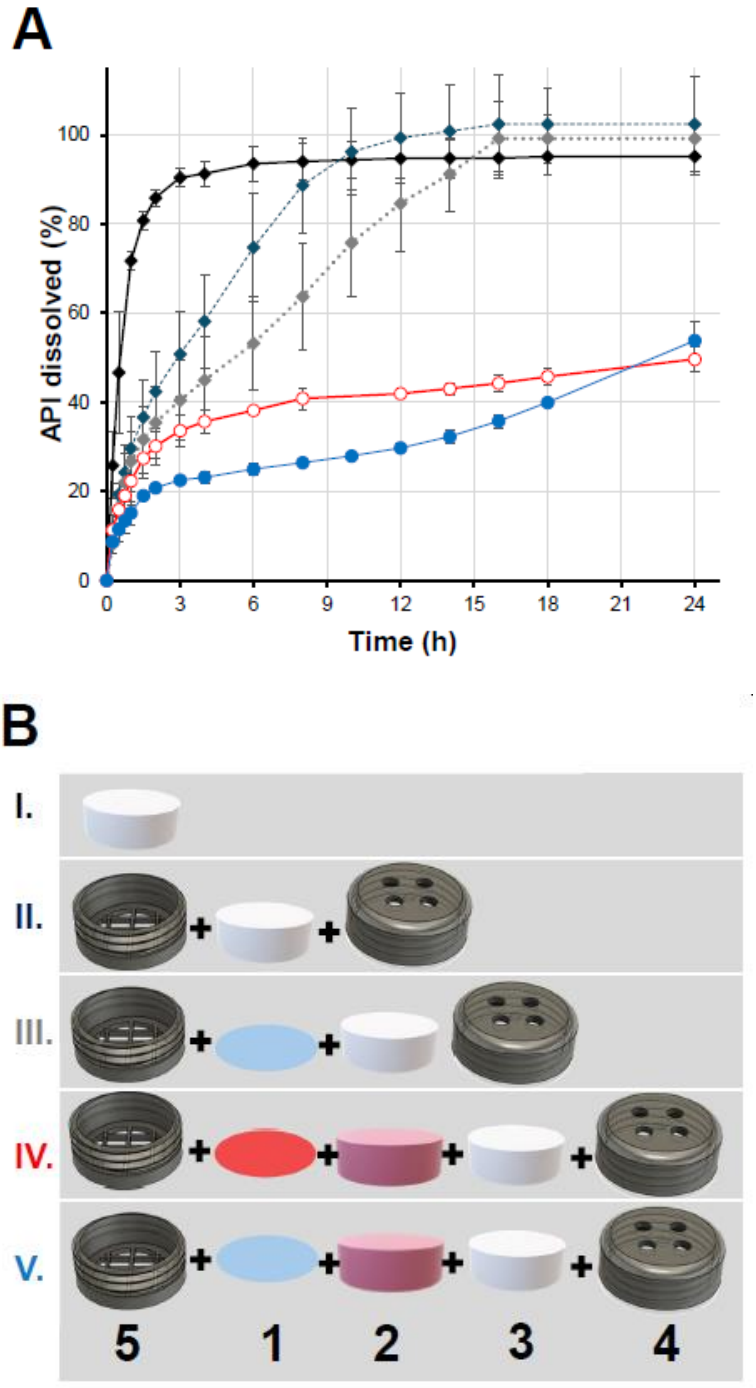

Figure 17: *A: dissolution studies of the formulations containing the assembled elements depicted in Figure 17 B, B: Elements of the assembled system (I.(black) pull tablet; II. (dark blue) two parts of the 3D printed frame and pull tablet; III. (grey) two parts of the 3D printed frame, pull tablet and membrane; IV. (red) two parts of the 3D printed frame, pull tablet, push tablet and membrane (A-25); V. (light blue) two parts of the 3D printed frame, pull tablet, push tablet and membrane (B-25) [11]*

Formulation I in Figure 17 shows, that if the API containing pull layer was investigated alone, after the rapid initial wetting and swelling of the tablet, a gel barrier layer was formed on the surface of the tablet, because of the viscosity of the HPMC excipient. After the gel formation of the HPMC, the active substance was diffused through this barrier layer. Almost 90% of the quinine hydrochloride model API were released within the first 4 hours, which indicates a relatively fast dissolution rate compared to other assembled formulations. In the case of formulation I, the drug release was predominantly influenced by the solubility of quinine hydrochloride, in addition to the presence of Hypromellose and only the first-order model described the dissolution profile well enough ($R > 0.95$).

Dissolution profiles of the other formulations can be described with the Korsmeyer-Peppas model to characterize the kinetics throughout the whole 24-hour period. The kinetic analysis of the dissolutions is shown in Table VII.

In the instance of formulation II, the pull tablet was assembled with the two parts of the additively manufactured frame, which had a constant internal volume. Compared with the dissolution of formulation I, the drug release was extended because the API containing pull tablet does not come into direct contact with the dissolution medium; thus, the medium must enter the frame to contact the tablet. The medium can enter the frame relatively quickly through the bottom part of the frame, since there is no membrane inserted into the system, which can block the ingress of the water, or through the drug delivery orifices designed on the upper part of the 3D printed frame. Once a sufficient amount of liquid is ingressed into the central cavity of the formulation, the wetting, the swelling, the hydration and the gelation of the HPMC polymer take place; however, unlike the previous case, the solid 3D printed frame restricts the gel layer from forming consistently across all directions. The release profile of formulation II was slower than it was for formulation I, but no zero-order release kinetics had formed yet.

If a semipermeable membrane was inserted into the 3D printed frame beside the pull layer, the ingress of water into the frame was slowed down from the direction of the bottom part. The dissolution of the active substance was shown an initial burst phase, but after that, the zero-order release kinetics may provide a prolonged and more predictable API release from the drug delivery systems, which contained semipermeable membranes compared to formulation I.

In the case of formulation IV and V, the push layer was used in the assemble of the drug delivery systems, the fixed volume provided by the frame and the push layer inhibits the swelling of the pull layer, however the wetted push layer swells, exerts pressure and the release of the active substance is initiated through the drug delivery orifices. The zero-order kinetics was estimated as the terminal phase of the dissolution, taking the second-hour sampling time as the first point of the linear regression stage following the medium replacement into consideration (Figures 17 and 18). The increased control of the system was also indicated by the decrease in the standard deviation values.

Table VII: The kinetic analysis of the dissolution of the different formulations (depicted in Figure 4.) containing assembled elements.

Model	Equation	First point of fitting	Sample	R	Parameters
Zero-order	$Q = kt + Q_{2h}$	2 hours	I	0.8098	$k = 0.4837$ %/h; $Q_{2h}= 88.593$ %
			II	0.9425	$k = 4.429$ %/h; $Q_{2h}= 42.381$ %
			III	0.9980	$k = 4.669$ %/h; $Q_{2h}=26.462$ %
			IV	0.9598	$k = 0.7817$ %/h; $Q_{2h}= 32.046$ %
			V	0.9662	$k = 1.3457$ %/h; $Q_{2h}=16.336$ %
First-order	$\ln(100 - Q) = -kt + \ln(100)$	0 hour	I	0.9970	$k = 1.146\ h^{-1}$
			II	0.9940	$k = 0.2690\ h^{-1}$
			III	0.9856	$k = 0.1641\ h^{-1}$
			IV	0.8706	$k = 0.\ 0475 h^{-1}$
			V	0.9396	$k = 0.0335\ h^{-1}$
Higuchi	$Q = k\sqrt{t}$	0 hour	I	0.7580	$k = 0.2829$ %/$h^{-1/2}$
			II	0.9712	$k = 0.2632$ %/$h^{-1/2}$
			III	0.9905	$k = 0.2312$ %/$h^{-1/2}$
			IV	0.9325	$k = 0.1257$ %/$h^{-1/2}$
			V	0.9623	$k = 0.0992$ %/$h^{-1/2}$

Model	Equation	First point of fitting	Sample	R	Parameters
Korsmeyer-Peppas	$Q = kt^n$	0 hour	I	0.8381	$k = 0.6605\ \%/h^n$; n = 0.1488
			II	0.9790	$k = 0.3411\ \%/h^n$; n = 0.4204
			III	0.9913	$k = 0.2535\ \%/h^n$; n = 0.4628
			IV	0.9752	$k = 0.2728\ \%/h^n$; n= 0.1805
			V	0.9631	$k = 0.1388\ \%/h^n$; n = 0.3622

The membrane compositions and casting temperature of the different membranes can affect the release of the API from the various drug delivery systems, as illustrated in Figure 18. According to the slopes and intercept values of the dissolution curves of drug delivery systems containing different membranes, the presence of glycerol in the membrane contributed to a slower initial API dissolution, but a faster zero-order release compared to the formulations, where only propylene glycol was used as a plasticizer. The membranes, prepared at 40°C, had approximately the same zero-order release rate (around 1%/ hour). Yet, membranes incorporating glycerol had a smaller initial burst release in comparison to membranes without glycerol, as it is shown in Figure 18. The addition of glycerol as a plasticizer enhances the films' wettability, as shown in Figure 10 and increases their water absorption capacity, as indicated in Table VI. This improvement leads to the formation of a thicker diffusion layer, which in turn reduces the water diffusion rate to the push layer and slows the drug release rate. In addition, the water-soluble propylene glycol dissolves on contact with the dissolution liquid and creates pores, thus the penetration of the water into the frame becomes easier. This aids the release of the API from the tablet.

With the prolonged, zero-order release rate of the novel osmotic release tablets, the individualized, patient centric dosing regimen can be introduced related to absorption rate-limited elimination.

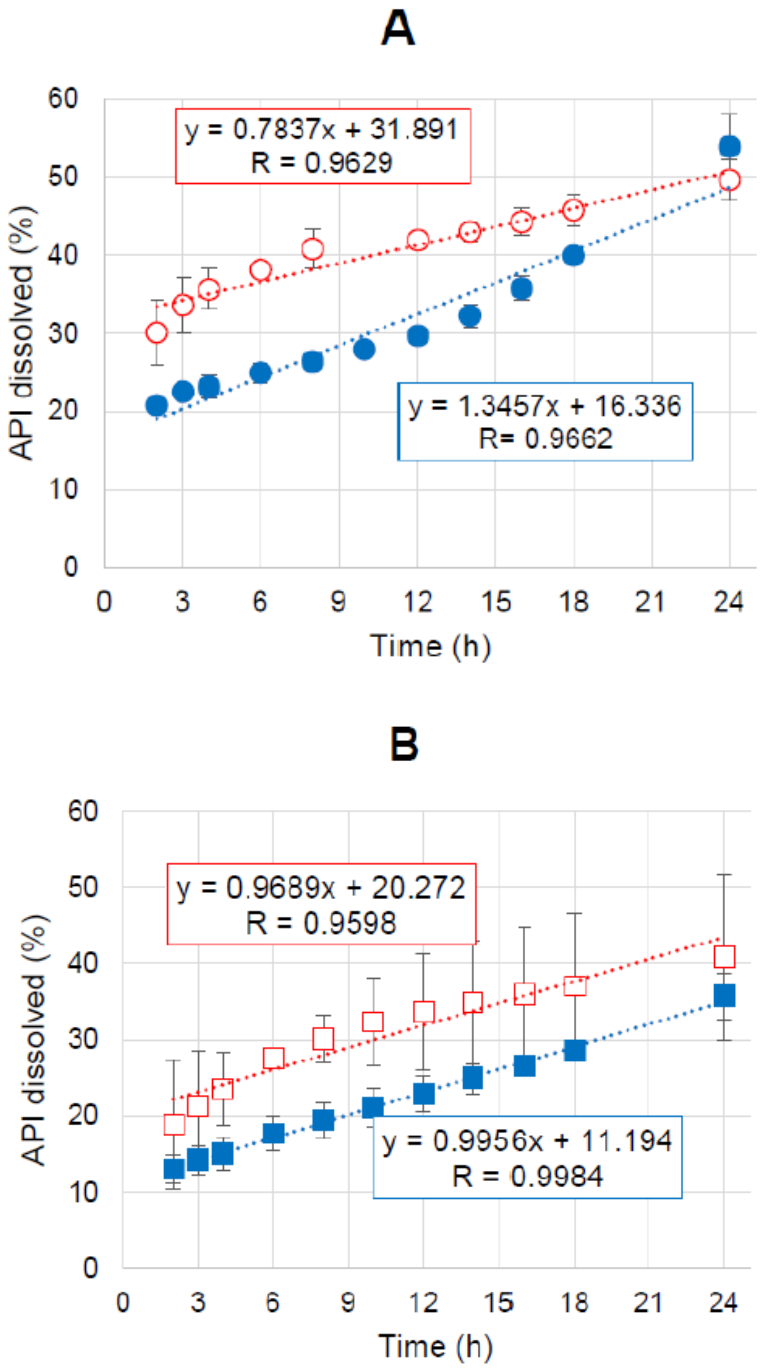

Figure 18: *A: Fitted points on the profile of API release from assembled prototype tablet (pull tablet, push tablet in a 3D printed frame, with A-25 membrane (red) and B-25 membrane (blue) produced at room temperature, B: Fitted points on the profile of API release from assembled prototype tablet (pull tablet, push tablet in a 3D printed frame, with A-40 membrane (red) and B-40 membrane (blue) produced at 40°C. [11]*

One of the major advantages of the OROS formulations, that their drug release is generally independent of the agitation intensity of the dissolution medium [39, 44, 76]. One of the aims of the current research was to verify that the desired zero-order release of the drug was not affected by the agitation speed; therefore, the dissolution was also investigated at various rotation speeds (rpm: 75/100/125) of the paddle. The dissolution profiles of the API in different revolution speeds are shown in Figure 19. It was experienced that the zero-order release of the innovative delivery system is independent of the agitation intensity. The values of the coefficients in the equation of the line fitted to the measured points are practically unchanged.

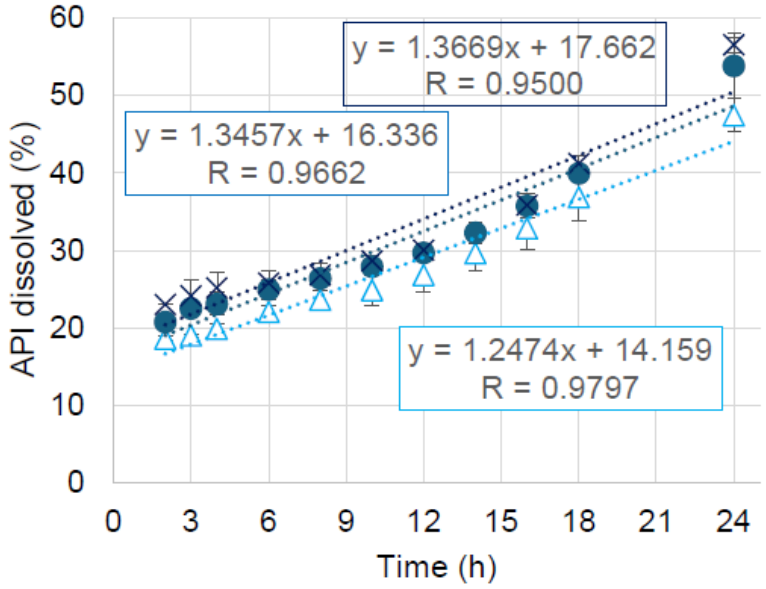

Figure 19: *Fitted release profiles of API from assembled prototype tablet at revolution rates of 125 rpm (triangle), 100 rpm (circle and 75 rpm(X) [11]*

4.2. Potential applicability of AM in dry media ball milling

4.2.1. Fabrication of the printlets

Among the various AM methods, the SLA technique was chosen for the printing of the model grinding balls due to the high resolution of the method. Because of this, not only can spherical balls be printed, but it also enables the opportunity to fabricate grinding balls of small sizes. In the future, it is a promising opportunity to print balls with less than 1 mm; thus, the micronization and nanonization with the additively manufactured milling

bodies can be performed. After the printing, a defined number of the milling balls was postcured. The CAD file and the pictures of the fabricated balls are shown in Figure 20.

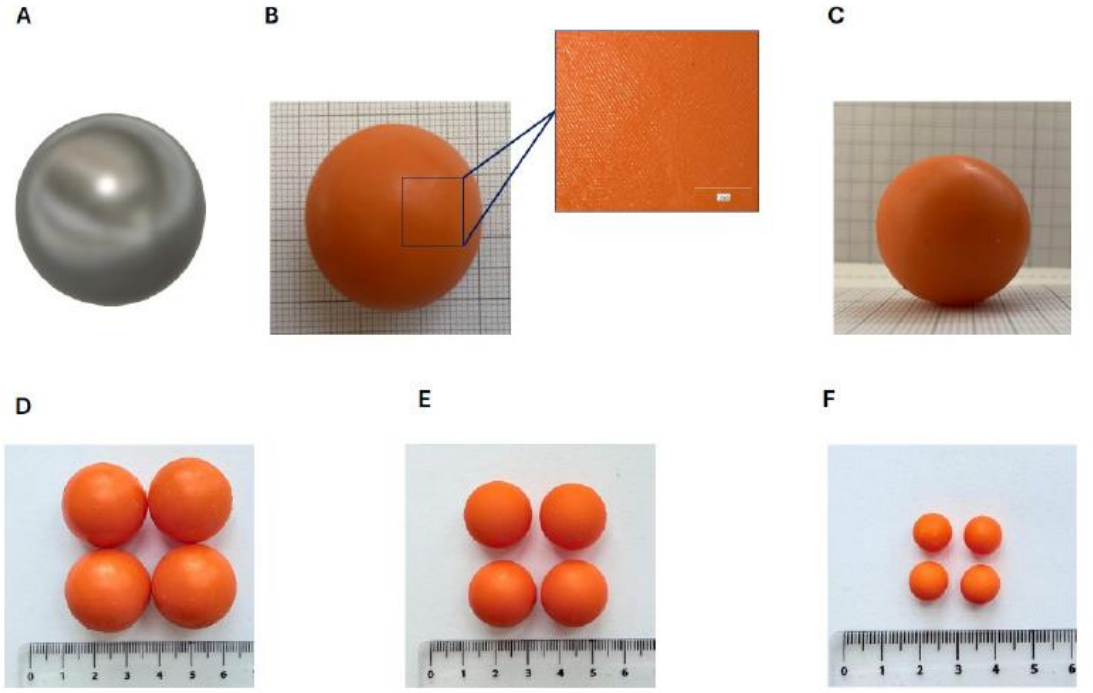

Figure 20: *Dry media milling balls fabricated with 3D printing ((**A**): The CAD file of the model, (**B**): Picture of the 3D printed milling ball (top view) and digital microscopic picture of the surface, (**C**): Picture of the 3D printed milling ball (side view), (**D**): Picture of the 3D printed balls (d= 25 mm), (**E**): Picture of the 3D printed balls (d= 20 mm), (**F**): Picture of the 3D printed balls (d = 10 mm) [72]*

4.2.2. Densities of the grinding balls

The size and mass of the different 3D printed, and conventional stainless-steel balls were measured, and the densities of the grinding bodies were calculated. The densities of both the stainless-steel balls and the 3D fabricated balls are nearly the same if we compare the grinding balls with the same material, but with different sizes. In every size, the comparator steel balls were denser than the 3D printed ones. The results are shown in Table VIII.

Table VIII: Densities of the grinding balls

Density of stainless-steel balls (g/cm3)	RSD (%)	Density of 3D printed balls (g/cm3)	RSD (%)
0.9642	0.01	0.1491	0.75
0.9620	0.01	0.1507	0.19
0.9649	0.04	0.1554	0.11

4.2.3. Weight loss test

The weight loss of the fabricated samples with and without postcuring was measured, and it was found to be negligible.

4.2.4 Particle size reduction

Particle size reduction with saccharose model material was executed in a planetary ball mill. The revolution speed was relatively low (200 rpm), and the implementation of break time into the procedure was necessary, due to the properties of the saccharose. Milling of the saccharose was performed at higher rotation speeds and without break time as well, although in these cases, the saccharose was partially melted when stainless steel balls were used as grinding media, which inhibited further particle size reduction and made the accurate particle size measurements impossible. Moreover, heat-sensitive materials can undergo structural modifications; therefore, lower milling rates and break times must be applied in case of dry media milling procedures. As the comparator of the 3D printed balls, conventional stainless-steel balls of the same size and aggregated ball mass were used. The results of particle size and particle size distribution studies are shown in Table IX.

It was experienced that the average particle size of the saccharose model material ground with 3D printed media was decreased more than in the case of the batch ground with a conventional stainless-steel ball. As Table IX shows, the more ball was used, the greater the decrease was experienced in the average particle size of the model material. The results were indicated that the postcuring of the fabricated milling balls resulted in improved milling efficiency. Based on the particle size distribution from the various processes, the SPAN values increased during milling with both stainless steel and with 3D fabricated balls, leading to a broader particle size distribution. The comparator

stainless steel balls provided the smallest change in particle size and the narrowest distribution both before and after the milling. Additively manufactured milling media balls were more effective at reducing the particle size; however, the particle size distribution of the saccharose was broader than in the case of the batch, milled with stainless steel balls. According to the findings from the prior particle size distribution studies, the SLA fabricated milling balls are effective for reducing particle size during dry media milling.

Table IX: Average particle size and SPAN values of the saccharose ground with different milling media

Grinding bodies	Initial/Milled	Average particle size (µm)	SD (µm)	SPAN	SD
Metal ball	initial	386.30	± 3.42	1.01	0.03
	milled	359.89	± 4.14	1.10	0.03
3D printed balls (6 pcs., with postcuring	initial	374.02	± 24.31	1.05	0.10
	milled	207.55	± 12.00	1.33	0.03
3D printed balls (4 pcs., with postcuring	initial	427.97	± 37.38	0.82	0.1
	milled	307.73	± 18.27	1.38	0.05
3D printed balls (4 pcs., without postcuring	initial	382.91	± 12.82	1.15	0.23
	milled	287.30	± 9.79	1.26	0.14

The digital microscopic pictures of the saccharose before and after milling with 3D printed balls were captured and are shown in Figure 21.

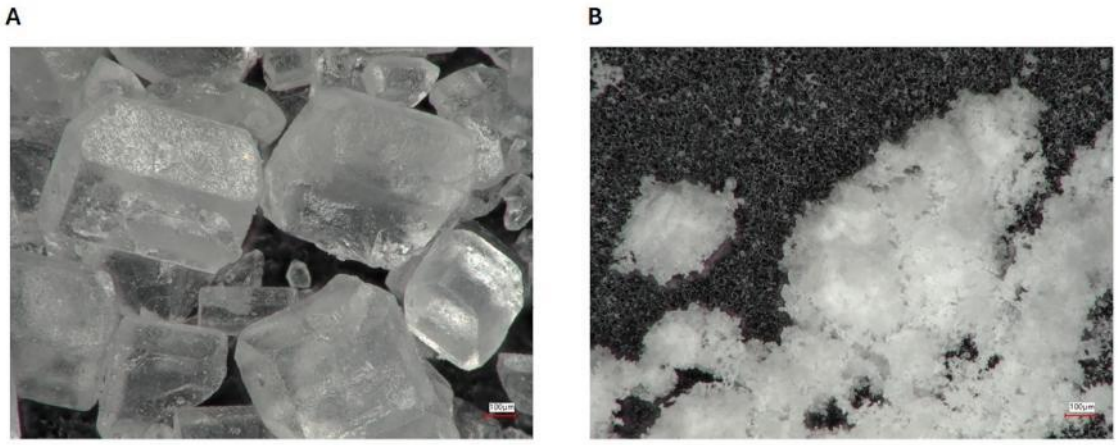

Figure 21: *Digital microscopic images of the saccharose, A: initial, B: after milling with additively manufactured balls [72]*

4.2.5. Warmup measurements in planetary ball mill

Thermal camera measurements:

The warmup of the 3D printed milling balls and the conventional stainless steel balls was investigated with a thermal camera. The rotation speed of the planetary ball mill was set to 400 rpm, and the elevation of the temperature was tracked within 45 minutes of the process. The thermal camera was automatically placed in the same position for every measurement, and it focused on the warmest point of the system automatically. The pictures, captured by the thermal camera, are shown in Figure 22. The initial temperature of the system was 30.5°C ± 0.5°C. Based on the results of the warmup tests, the additively manufactured grinding balls were heated up less than the comparator metal balls under the same conditions. The difference in the temperature of the systems between the additively manufactured balls and the conventional stainless steel ball was around 26 °C after 45 minutes procedure time. The temperature difference can explain the altered structural changes of heat-sensitive materials during dry media ball milling, between grinding with balls manufactured from different materials.

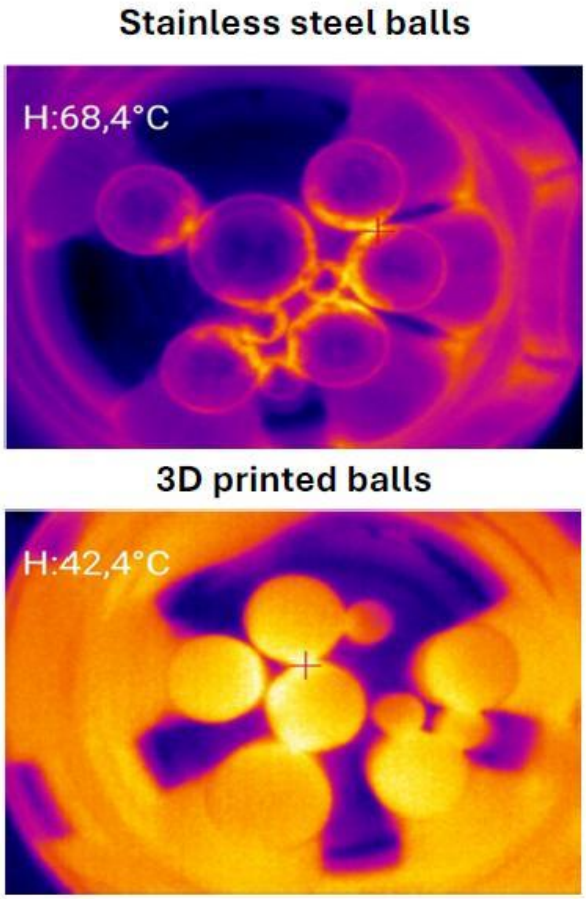

Figure 22: *Thermal camera images of the system [72].*

The effect of the warmup on lactose monohydrate:

Lactose monohydrate, as a model material was used to investigate the effect of the warmup during the dry media ball milling process on the structure of materials. Samples were collected after 45 minutes of grinding in the planetary ball mill. The samples were investigated with DSC. The thermogram of the initial, raw sample of lactose monohydrate ground for 45 minutes with stainless steel balls, and the sample of lactose monohydrate ground for 45 minutes with 3D fabricated milling balls were registered and shown in Figure 23. The intensity and the placements of the endothermic peak on the thermograms of the raw lactose monohydrate and the ground material were compared. The initial lactose monohydrate showed a sharp endothermic peak at 148.9 °C, which refers to the loss of the crystalline water [77]. The sample ground with 3D printed balls showed no significant structural alterations, since the endothermic peak was retained at 148.9 °C

with similar sharpness. However, the position of the peak in the thermogram of the sample milled with metal balls altered to 134.7 °C, and it exhibited a broadened peak, indicating partial amorphization or destabilization of the crystal lattice caused by heat-induced stress. The friction-induced increased warmup during the milling with metal balls likely caused the thermal degradation and modification of the lactose's crystalline structures, which results align well with the results of the thermal camera measurements.

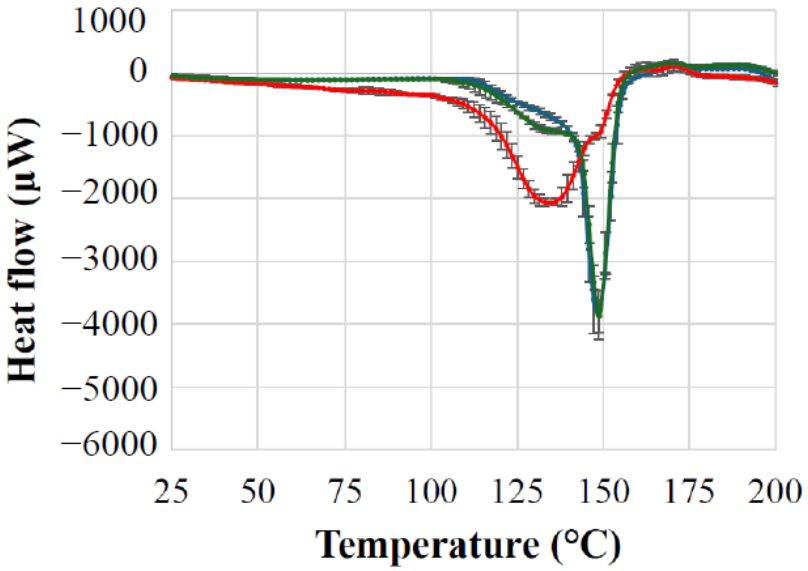

Figure 23: *DSC thermograms of the lactose monohydrate samples (blue: initial lactose monohydrate, green: thermogram after grinding with 3D printed balls, red: thermogram after milling with stainless steel balls) [72]*

5. Discussion

The AM is considered a flexible tool with various possible applications. During the current research, it is a promising method, that can be used in the formulation of innovative drug delivery systems with tailored drug delivery. Taking the easy and quick modifiability of the system into consideration, 3D printing can be applied to personalised medication on a daily basis, revolutionising drug therapies.

This thesis presents a prototype for a modified-release osmotic release tablet, where the complex system was designed and assembled from different components. Although the idea of utilizing the AM in the fabrication of modular, multi-compartment drug delivery systems is not novel, the combination of the 3D printing techniques with the traditional pharmaceutical technology methods and the utilization of AM in the fabrication of an OROS-type tablet reflects a key innovation in the field. The created delivery system has the opportunity for precise tailoring of the drug release mechanisms and control over the release profile; thus, the drug delivery can meet the unique needs of the patients in human and veterinary applications. The compositions the properties of the different parts of the osmotic delivery system, akin to Lego® blocks can be dynamically changed, and with the quick modification of the 3D printed frame, the therapies can achieve a better individualisation. Since the modification of the 3D printed frame is quick and does not require special, extra equipment, they can also be carried out in hospital pharmacies. In light of the results of the thesis, I see merit in the future integration of AM into the everyday practices of institutional pharmacies, which can improve the effectiveness of the treatments.

The results show that the different membrane compositions formulated at different temperatures have different properties, which influence the final drug delivery of the assembled complex system. The in vitro dissolution profiles of the systems, which contained various elements (3D printed frame, semipermeable membrane, push, pull layer), had different dissolution profiles. The results showed that the application of cellulose acetate membranes is essential to obtain zero-order kinetic release.

The 3D printing can also be utilized to fabricate dry media milling balls with low densities, which can be alternatives to metal balls in a conventional base operation, grinding. The unique approach of using 3D printed balls in the milling process, measuring their efficiency in the particle size reduction, and examining the warmup of the system

can be a basis of future research in the material sciences, and it can revolutionise the grinding in the pharmaceutical industries, thus it represents a significant advancement in the field.

The results show that the warmup of the system during the tests with additively manufactured grinding balls was much lower than it was if the tests were performed with conventional stainless steel balls. This advantage of the 3D fabricated milling balls gives the opportunity to the pharmaceutical industry to use higher milling rates, and the application of break time during the process is not required; thus, the total procedure time can be decreased. Furthermore, the utilization of 3D printed grinding balls is considered to be safer in the case of grinding heat-sensitive materials, amorphization or degradation of these materials can be avoided. This approach could result in a more efficient, optimized, time-consuming and cost-effective method for pharmaceutical companies to adopt.

According to the findings of the thesis, the more extensive future application of the AM in the hospital pharmacies and in the industrial pharmaceutical companies can offer very promising and beneficial opportunities. The high flexibility of the methods ensures that this tool is effective in both basic manufacturing operations and personalized, modern drug therapies. In the future, with the development of the materials sciences, the formulation of more biocompatible resins for SLA printing will be a huge milestone for the translation of this concept.

6. Conclusion

- The thesis proved that stereolithography (SLA) 3-D printing can be combined with compression units to fabricate complex, push–pull-type osmotic tablets that meet European Pharmacopoeia quality requirements. A modular, “Lego-like” frame printed by SLA allowed easy assembly and rapid design iterations; by simply exchanging individual blocks (push layer, pull layer, semipermeable film), drug release kinetics could be tuned without altering the API blend or compression protocol.
- Four cellulose-acetate membrane recipes were optimised: plasticiser composition (propylene glycol ± glycerol), casting temperature (25 °C vs 40 °C) and thickness (50–250 µm) all influenced water uptake, contact angle, pore formation and therefore osmotic pumping rate.
- Membranes containing a dual plasticiser system (CA:PG:GLY = 1:1:1) cast at 25 °C (B-25) showed the highest water content (11.2 ± 0.6%) and permeability, yielding the most constant zero-order release.
- Optimised push tablets (quinine HCl 25% w/w) and pull tablets (NaCl 25% w/w) were compressed separately, passed mass, hardness, friability and dimensional tests, and together generated the hydrostatic pressure needed for a robust push–pull mechanism.
- Dissolution studies in USP II paddles (75–125 rpm, pH 1.2 and 6.8) confirmed agitation-independent, zero-order release from the second hour of the dissolution test; linear regression coefficients exceeded 0.95 and standard deviations fell markedly after modular assembly.
- 3-D printed resin grinding balls were successfully employed in planetary ball milling of saccharose, lowering median particle size from 374 µm to 208 µm within 15 min—despite a density six-times lower than stainless steel—highlighting the customisability and cost savings of printed media.
- The warmup of the system with additively manufactured balls was lower than in the case of conventional stainless steel grinding bodies, which is exceptionally beneficial in the instance of the comminution of heat-sensitive materials. The results of the DSC measurements of the lactose dry milling aligned well with this phenomenon.

- Overall, additive manufacturing delivered a flexible, scalable and cost-effective platform that:
  – enables patient-tailored dose and release profiles without retooling;
  – reduces material waste by on-demand production;
  – integrates easily with existing pharmaceutical unit operations;
  – opens new avenues for personalised, zero-order controlled-release medicines and bespoke milling equipment in the pharmaceutical industry.

7. Summary

In the first phase of my doctoral research, the application opportunities of the AM in the field of the formulation of modular drug delivery systems were investigated. The SLA technique over the other 3D printing methods due to the high resolution of the tool was chosen. The Raydent Crown & Bridge resin was chosen during the AM of the printlets because of the higher biocompatibility of the material compared to other SLA resins. During the experiments, the elements of the complex osmotic release drug delivery system were optimized, and the delivery systems from the 3D printed frame and the conventionally manufactured elements were successfully assembled. The measurements justified that the tablets, which contained different elements, had different dissolution profiles; thus, the drug delivery can be modified and tailored to the patients' needs. With the insertion of the push, pull and semipermeable membrane into the 3D printed frame, after an initial burst phase in the dissolution profile, a zero-order release was established from the second hour of the in vitro dissolution studies. Due to this release, the blood level of the API in the patient is going to be more consistent, and because of the prolonged release of the innovative drug delivery system, the dosing regimen suits the patients' preferences better than an IR tablet.

The second phase of the research aimed at the exploration of the potential applicability of the resin-based printing in one of the basic processes of the pharmaceutical technology, the dry media ball milling. The analysis of the scientific literature demonstrated that one of the main limitations of dry milling is the warmup of the system caused by the collisions of the conventional metal-based grinding media and the grinding jar. Milling balls with the SLA technique were successfully printed, and these printed grinding bodies were suitable for the comminution method. The warmup tests, where additively manufactured milling balls were utilized, showed moderate warmup compared to the conventionally used stainless steel comparator medium.

Based on all the results, the AM can be a promising tool in revolutionizing the pharmaceutical base operations in the industrial environments, and the patient centric therapeutic approaches as well by the implementation of these techniques into the everyday practices of the hospital pharmacies.

8. References

1. Vaz, V.M.,L. Kumar, *3D Printing as a Promising Tool in Personalized Medicine.* AAPS PharmSciTech, 2021. **22**(1): p. 49 DOI: 10.1208/s12249-020-01905-8.
2. Melocchi, A., M. Uboldi, A. Maroni, A. Foppoli, L. Palugan, L. Zema,A. Gazzaniga, *3D printing by fused deposition modeling of single- and multi-compartment hollow systems for oral delivery – A review.* International Journal of Pharmaceutics, 2020. **579**: p. 119155 DOI: https://doi.org/10.1016/j.ijpharm.2020.119155.
3. Ameta, K.L., V.S. Solanki, V. Singh, A.P. Devi, R.S. Chundawat,S. Haque, *Critical appraisal and systematic review of 3D & 4D printing in sustainable and environment-friendly smart manufacturing technologies.* Sustainable Materials and Technologies, 2022. **34**: p. e00481 DOI: https://doi.org/10.1016/j.susmat.2022.e00481.
4. Goyanes, A., P. Robles Martinez, A. Buanz, A.W. Basit,S. Gaisford, *Effect of geometry on drug release from 3D printed tablets.* International Journal of Pharmaceutics, 2015. **494**(2): p. 657-663 DOI: https://doi.org/10.1016/j.ijpharm.2015.04.069.
5. Lafeber, I., E.J. Ruijgrok, H.-J. Guchelaar,K.J.M. Schimmel, *3D Printing of Pediatric Medication: The End of Bad Tasting Oral Liquids?-A Scoping Review.* Pharmaceutics, 2022. **14**(2): p. 416 DOI: 10.3390/pharmaceutics14020416.
6. Korte, C.,J. Quodbach, *3D-Printed Network Structures as Controlled-Release Drug Delivery Systems: Dose Adjustment, API Release Analysis and Prediction.* AAPS PharmSciTech, 2018. **19**(8): p. 3333-3342 DOI: 10.1208/s12249-018-1017-0.
7. Karavasili, C., G.K. Eleftheriadis, C. Gioumouxouzis, E.G. Andriotis,D.G. Fatouros, *Mucosal drug delivery and 3D printing technologies: A focus on special patient populations.* Advanced Drug Delivery Reviews, 2021. **176**: p. 113858 DOI: https://doi.org/10.1016/j.addr.2021.113858.
8. Zhu, X., H. Li, L. Huang, M. Zhang, W. Fan,L. Cui, *3D printing promotes the development of drugs.* Biomedicine & Pharmacotherapy, 2020. **131**: p. 110644 DOI: https://doi.org/10.1016/j.biopha.2020.110644.

9. Zheng, Z., J. Lv, W. Yang, X. Pi, W. Lin, Z. Lin, W. Zhang, J. Pang, Y. Zeng, Z. Lv, H. Lao, Y. Chen,F. Yang, *Preparation and application of subdivided tablets using 3D printing for precise hospital dispensing.* European Journal of Pharmaceutical Sciences, 2020. **149**: p. 105293 DOI: https://doi.org/10.1016/j.ejps.2020.105293.
10. Basa, B., G. Jakab, N. Kállai-Szabó, B. Borbás, V. Fülöp, E. Balogh,I. Antal *Evaluation of Biodegradable PVA-Based 3D Printed Carriers during Dissolution*. Materials, 2021. **14**, DOI: 10.3390/ma14061350.
11. Borbás, B., N. Kállai-Szabó, M. Lengyel, E. Balogh, B. Basa, K. Süvegh, R. Zelkó,I. Antal, *Microfabrication of controlled release osmotic drug delivery systems assembled from designed elements.* Expert Opinion on Drug Delivery: p. 1-13 DOI: 10.1080/17425247.2024.2412826.
12. Lamichhane, S., S. Bashyal, T. Keum, G. Noh, J.E. Seo, R. Bastola, J. Choi, D.H. Sohn,S. Lee, *Complex formulations, simple techniques: Can 3D printing technology be the Midas touch in pharmaceutical industry?* Asian Journal of Pharmaceutical Sciences, 2019. **14**(5): p. 465-479 DOI: https://doi.org/10.1016/j.ajps.2018.11.008.
13. Khalid, G.M.,N. Billa *Solid Dispersion Formulations by FDM 3D Printing—A Review*. Pharmaceutics, 2022. **14**, DOI: 10.3390/pharmaceutics14040690.
14. Doshi, M., A. Mahale, S. Kumar Singh,S. Deshmukh, *Printing parameters and materials affecting mechanical properties of FDM-3D printed Parts: Perspective and prospects.* Materials Today: Proceedings, 2022. **50**: p. 2269-2275 DOI: https://doi.org/10.1016/j.matpr.2021.10.003.
15. Brambilla, C.R.M., O.L. Okafor-Muo, H. Hassanin,A. ElShaer *3DP Printing of Oral Solid Formulations: A Systematic Review*. Pharmaceutics, 2021. **13**, DOI: 10.3390/pharmaceutics13030358.
16. Mathew, E., G. Pitzanti, E. Larrañeta,D.A. Lamprou *3D Printing of Pharmaceuticals and Drug Delivery Devices*. Pharmaceutics, 2020. **12**, DOI: 10.3390/pharmaceutics12030266.
17. Ogochukwu, L.O.-M., H. Hany, K. Reem,E. Amr, *3D Printing of Solid Oral Dosage Forms: Numerous Challenges With Unique Opportunities.* Journal of Pharmaceutical Sciences, 2020. **109**(12): p. 3535-3550.

18. Husna, A., S. Ashrafi, A.N.M.A. Tomal, N.T. Tuli,A. Bin Rashid, *Recent advancements in stereolithography (SLA) and their optimization of process parameters for sustainable manufacturing.* Hybrid Advances, 2024. **7**: p. 100307 DOI: https://doi.org/10.1016/j.hybadv.2024.100307.
19. Jamróz, W., J. Szafraniec, M. Kurek,R. Jachowicz, *3D Printing in Pharmaceutical and Medical Applications – Recent Achievements and Challenges.* Pharmaceutical Research, 2018. **35**(9): p. 176 DOI: 10.1007/s11095-018-2454-x.
20. Pereira, B.C., A. Isreb, M. Isreb, R.T. Forbes, E.F. Oga,M.A. Alhnan, *Additive Manufacturing of a Point-of-Care "Polypill:" Fabrication of Concept Capsules of Complex Geometry with Bespoke Release against Cardiovascular Disease.* Advanced Healthcare Materials, 2020. **9**(13): p. 2000236 DOI: https://doi.org/10.1002/adhm.202000236.
21. Lu, A., J. Zhang, J. Jiang, Y. Zhang, B.R. Giri, V.R. Kulkarni, N.H. Aghda, J. Wang,M. Maniruzzaman, *Novel 3D Printed Modular Tablets Containing Multiple Anti-Viral Drugs: a Case of High Precision Drop-on-Demand Drug Deposition.* Pharmaceutical Research, 2022. **39**(11): p. 2905-2918 DOI: 10.1007/s11095-022-03378-9.
22. Melocchi, A., M. Uboldi, F. Parietti, M. Cerea, A. Foppoli, L. Palugan, A. Gazzaniga, A. Maroni,L. Zema, *Lego-Inspired Capsular Devices for the Development of Personalized Dietary Supplements: Proof of Concept With Multimodal Release of Caffeine.* Journal of Pharmaceutical Sciences, 2020. **109**(6): p. 1990-1999 DOI: https://doi.org/10.1016/j.xphs.2020.02.013.
23. Govender, R., S. Abrahmsén-Alami, A. Larsson, A. Borde, A. Liljeblad,S. Folestad *Independent Tailoring of Dose and Drug Release via a Modularized Product Design Concept for Mass Customization*. Pharmaceutics, 2020. **12**, DOI: 10.3390/pharmaceutics12080771.
24. Antal, I., *Módosított hatóanyag-leadású szilárd gyógyszerformák szerkezetének és működésének összefüggései.* Studium&practicum, 2009: p. 4-10.
25. Kumar, J., C. Rao, R. Singh, A. Garg,R. Tanniru, *A Comprehensive Review on Modified-Release Tablets.* International Journal of Newgen Research in Pharmacy & Healthcare, 2024: p. 184-192 DOI: 10.61554/ijnrph.v2i2.2024.116.

26. Antal, I.,I. Klebovich, *A fájdalomterápia farmakokinetikán alapuló optimalizálása-innovatív hatóanyag-leadó rendszerek.* Lege Artis Medicinae, 2008. **18**(11): p. 783-789.
27. Kuchibhotla, N.S.S., M. Sunitha Reddy,A.K. Vijetha, *Delayed Release Pellets: A Comprehensive Review.* International Journal of Research Publication and Reviews, 2024. **5**(5): p. 12787-12795.
28. Singh, D., S. Poddar, S. Nigade,S. Poddar, *Pulsatile Drug Delivery System: An Overview.* International Journal of Current Pharmaceutical Review and Research, 2011. **2**.
29. Mal, M., M. Chakraborty,A. Datta, *EXTENDED RELEASE TABLET: REVIEW.* 2023: p. 2582-5208.
30. Lautenschläger, C., C. Schmidt, D. Fischer,A. Stallmach, *Drug delivery strategies in the therapy of inflammatory bowel disease.* Advanced Drug Delivery Reviews, 2014. **71**: p. 58-76 DOI: https://doi.org/10.1016/j.addr.2013.10.001.
31. Djamel, G., *Reverse Osmosis Process Membranes Modeling – A Historical Overview.* Journal of Civil, Construction and Environmental Engineering, 2017. **2**(4): p. 112-122 DOI: 10.11648/j.jccee.20170204.12.
32. Damjanovich, S., J. Fidy,J. Szöllősi, *Orvosi Biofizika*. 2007, Budapest: Medicina Könyvkiadó Zrt. .
33. Santus, G.,R.W. Baker, *Osmotic drug delivery: a review of the patent literature.* Journal of Controlled Release, 1995. **35**(1): p. 1-21 DOI: https://doi.org/10.1016/0168-3659(95)00013-X.
34. Thakor, R.S., F.D. Majmudar, J.K. Patel,G.C. Rajaput, *Review: Osmotic drug delivery system current scenario.* Journal of Pharmacy Research, 2010. **34**: p. 771-775.
35. Tanmoy, G.,G. Amitava, *Drug Delivery Through Osmotic Systems- An Overview.* Journal of Applied Pharmaceutical Science, 2011. **01**(02): p. 38-49.
36. Nikam, P.H., J.A. Kareparamban, A.p. Jandav,V.J. Kadam, *Osmotic Pump: A Reliable Drug Delivery System.* Research Journal of Pharmaceutical, Biological and Chemical Sciences, 2012. **3**(3): p. 478-493.

37. Gupta, B.P., N. Thakur, N.P. Jain, J. Banweer,S. Jain, *Osmotically controlled drug delivery system with associated drugs.* J Pharm Pharm Sci, 2010. **13**(4): p. 571-88 DOI: 10.18433/j38w25.

38. Samar, M., H.N. Saydeh, M. Salar, K. Shalen,G. Tooba, *A Review of Osmotic Pump Applications as a Reliable Drug Delivery System in Pharmaceutical Sciences.* Biomedical Research Bulletin, 2024. **2**(1): p. 29-36.

39. Keraliya, R.A., C. Patel, P. Patel, V. Keraliya, T.G. Soni, R.C. Patel,M.M. Patel, *Osmotic Drug Delivery System as a Part of Modified Release Dosage Form.* International Scholarly Research Notices, 2012. **2012**(1): p. 528079 DOI: https://doi.org/10.5402/2012/528079.

40. Patil, P.B., K.B. Uphade,R.B. Saudagar, *A Review: Osmotic Drug Delivery System.* An International Journal Of Pharmaceutical Sciences, 2018. **9**(2): p. 283-300.

41. Qin, C., W. He, C. Zhu, M. Wu, Z. Jin, Q. Zhang, G. Wang,L. Yin, *Controlled release of metformin hydrochloride and repaglinide from sandwiched osmotic pump tablet.* International Journal of Pharmaceutics, 2014. **466**(1): p. 276-285 DOI: https://doi.org/10.1016/j.ijpharm.2014.03.002.

42. Yang, C., X. Ji, W. Pan, Y. Liu, L. Zhou, Q. Chen,X. Tang, *Paliperidone ascending controlled-release pellets with osmotic core and driven by delayed osmotic pressure.* Journal of Drug Delivery Science and Technology, 2018. **48**: p. 193-199 DOI: https://doi.org/10.1016/j.jddst.2018.09.018.

43. Prasanna, N., C. Srilatha,C.V.S. Subrahmanyam, *Osmotic Controlled Release Oral Delivery System: An Overview.* International Journal of Pharmaceutical Sciences, 2024. **2**(3): p. 530-558.

44. Almoshari, Y. *Osmotic Pump Drug Delivery Systems—A Comprehensive Review*. Pharmaceuticals, 2022. **15**, DOI: 10.3390/ph15111430.

45. Mene, H.R., N.R. Mene, D.R. Parakh, T.B. Ingale, D.R. Magar,M.R. Mangale, *Formulation aspects in development of controlled porosity osmotic pump tablet.* Pharmaceutical and Biological Evaluations, 2016. **3**(1): p. 1-18.

46. Verma, R.K., D.M. Krishna,S. Garg, *Formulation aspects in the development of osmotically controlled oral drug delivery systems.* Journal of Controlled Release, 2002. **79**(1): p. 7-27 DOI: https://doi.org/10.1016/S0168-3659(01)00550-8.

47. Ahuja, N., V. Kumar,P. Rathee, *Osmotic-Controlled Release Oral Delivery System: An Advanced Oral Delivery Form.* The Pharma Innovation, 2012. **1**(7): p. 116-124.
48. Patel, J., S. Parikh,S. Patel, *COMPREHENSIVE REVIEW ON OSMOTIC DRUG DELIVERY SYSTEM.* World Journal of Pharmaceutical Research, 2021. **10**: p. 523-550 DOI: 10.20959/wjpr20215-20303.
49. Chourasia, P., S. Fr, H. Pardhe,H. Lodh, *A Comprehensive Review on Osmotic Controlled Drug Delivery System.* American Journal of PharmTech Research, 2020. **10**: p. 92-113 DOI: 10.46624/ajptr.2020.v10.i1.009.
50. Malaterre, V., J. Ogorka, N. Loggia,R. Gurny, *Oral osmotically driven systems: 30 years of development and clinical use.* European Journal of Pharmaceutics and Biopharmaceutics, 2009. **73**(3): p. 311-323 DOI: https://doi.org/10.1016/j.ejpb.2009.07.002.
51. Shoaeb, M.S., Z. Farooqui, M. Mohammed, K. Dureshahwar,M. Farooqui, *Osmotic Drug Delivery System: An Overview.* International Journal of Pharmaceutical Research & Allied Sciences, 2015. **4**(3): p. 10-20.
52. Amidon, G.E., P.J. Secreast,D. Mudie, *Chapter 8 - Particle, Powder, and Compact Characterization*, in *Developing Solid Oral Dosage Forms*, Y. Qiu, et al., Editors. 2009, Academic Press: San Diego. p. 163-186.
53. Nakach, M., J.-R. Authelin, A. Chamayou,J. Dodds, *Comparison of various milling technologies for grinding pharmaceutical powders.* International Journal of Mineral Processing, 2004. **74**: p. S173-S181 DOI: https://doi.org/10.1016/j.minpro.2004.07.039.
54. Bentham, A.C., C.C. Kwan, R. Boerefijn,M. Ghadiri, *Fluidised-bed jet milling of pharmaceutical powders.* Powder Technology, 2004. **141**(3): p. 233-238 DOI: https://doi.org/10.1016/j.powtec.2004.01.024.
55. Patel, R.P., A.H. Baria,N.A. Patel, *An overview of size reduction technologies in the field of pharmaceutical manufacturing.* Asian Journal of Pharmaceutics (AJP), 2014. **2**(4) DOI: 10.22377/ajp.v2i4.202.
56. Matsanga, N., W. Nheta,N. Chimwani *A Review of the Grinding Media in Ball Mills for Mineral Processing*. Minerals, 2023. **13**, DOI: 10.3390/min13111373.

57. Li, P., Z. Cao, R. Zhao, G. Li, M. Yu,S. Zhang, *The kinetics and efficiency of batch ball grinding with cemented tungsten carbide balls.* Advanced Powder Technology, 2020. **31**(6): p. 2412-2420 DOI: https://doi.org/10.1016/j.apt.2020.04.007.
58. Zhang, X., Y. Han,S. Kawatra, *Effects of Grinding Media on Grinding Products and Flotation Performance of Sulfide Ores.* Mineral Processing and Extractive Metallurgy Review, 2020. **42**: p. 1-12 DOI: 10.1080/08827508.2019.1692831.
59. Guner, G., H. Heidari, K. Lehman, P.M. Desai, D. Clancy, E. Bilgili,S. Chattoraj, *Comparative analysis of polystyrene versus zirconia beads on breakage kinetics, heat generation, and amorphous formation during wet bead milling.* Journal of Pharmaceutical Sciences, 2025. **114**(2): p. 1175-1185 DOI: https://doi.org/10.1016/j.xphs.2024.11.029.
60. Memarvar, D., S. Yaqoubi, H. Hamishehkar, M. Lam,A. Nokhodchi, *Impact of grinding balls on the size reduction of Aprepitant in wet ball milling procedure.* Pharmaceutical Development and Technology, 2024. **29**(4): p. 353-358 DOI: 10.1080/10837450.2024.2334754.
61. Zhang, J., Y. Bai, H. Dong, Q. Wu,X. Ye, *Influence of ball size distribution on grinding effect in horizontal planetary ball mill.* Advanced Powder Technology, 2014. **25**(3): p. 983-990 DOI: https://doi.org/10.1016/j.apt.2014.01.018.
62. AmanNejad, M.,K. Barani, *Effects of Ball Size Distribution and Mill Speed and Their Interactions on Ball Milling Using DEM.* Mineral Processing and Extractive Metallurgy Review, 2021. **42**(6): p. 374-379 DOI: 10.1080/08827508.2020.1781630.
63. Canakci, A., F. Erdemir, T. Varol,A. Patir, *Determining the effect of process parameters on particle size in mechanical milling using the Taguchi method: Measurement and analysis.* Measurement, 2013. **46**(9): p. 3532-3540 DOI: https://doi.org/10.1016/j.measurement.2013.06.035.
64. Knieke, C., M. Sommer,W. Peukert, *Identifying the apparent and true grinding limit.* Powder Technology, 2009. **195**(1): p. 25-30 DOI: https://doi.org/10.1016/j.powtec.2009.05.007.
65. Chen, Y., X. Lian, Z. Li, S. Zheng,Z. Wang, *Effects of rotation speed and media density on particle size distribution and structure of ground calcium carbonate in*

a planetary ball mill. Advanced Powder Technology, 2015. **26**(2): p. 505-510 DOI: https://doi.org/10.1016/j.apt.2014.12.007.

66. Watanabe, H., *Critical rotation speed for ball-milling.* Powder Technology, 1999. **104**(1): p. 95-99 DOI: https://doi.org/10.1016/S0032-5910(99)00031-5.
67. Descamps, M.,J.F. Willart, *Perspectives on the amorphisation/milling relationship in pharmaceutical materials.* Advanced Drug Delivery Reviews, 2016. **100**: p. 51-66 DOI: https://doi.org/10.1016/j.addr.2016.01.011.
68. Schmidt, R., H. Martin Scholze,A. Stolle, *Temperature progression in a mixer ball mill.* International Journal of Industrial Chemistry, 2016. **7**(2): p. 181-186 DOI: 10.1007/s40090-016-0078-8.
69. Loh, Z.H., A.K. Samanta,P.W. Sia Heng, *Overview of milling techniques for improving the solubility of poorly water-soluble drugs.* Asian Journal of Pharmaceutical Sciences, 2015. **10**(4): p. 255-274 DOI: https://doi.org/10.1016/j.ajps.2014.12.006.
70. Kotake, N., M. Kuboki, S. Kiya,Y. Kanda, *Influence of dry and wet grinding conditions on fineness and shape of particle size distribution of product in a ball mill.* Advanced Powder Technology, 2011. **22**(1): p. 86-92 DOI: https://doi.org/10.1016/j.apt.2010.03.015.
71. Suvegh, K., A. Vértes,T. Hyodo, *Positronium as a sensitive detector of changes in molecular structure.* Advances in Molecular Structure Research 1999. **5**: p. 313-358.
72. Borbás, B., Z. Kohod, N. Kállai-Szabó, B. Basa, M. Lengyel, R. Zelkó,I. Antal *Evaluation of 3D-Printed Balls with Photopolymer Resin as Grinding Medium Used to Alternatively Reduce Warmup During Dry Milling*. Polymers, 2025. **17**, DOI: 10.3390/polym17131795.
73. Prakash Maran, J., V. Sivakumar, R. Sridhar,V. Prince Immanuel, *Development of model for mechanical properties of tapioca starch based edible films.* Industrial Crops and Products, 2013. **42**: p. 159-168 DOI: https://doi.org/10.1016/j.indcrop.2012.05.011.
74. Suderman, N., M.I.N. Isa,N.M. Sarbon, *Effect of drying temperature on the functional properties of biodegradable CMC-based film for potential food packaging.* International Food Research Journal, 2016. **23**(3): p. 1075-1084.

75. *<711> Dissolution. In: USP–NF. United States Pharmacopeia; 2023. DOI: 10.31003/USPNF_M99470_03_01.*

76. Liu, L., J. Ku, G. Khang, B. Lee, J.M. Rhee,H.B. Lee, *Nifedipine controlled delivery by sandwiched osmotic tablet system.* Journal of Controlled Release, 2000. **68**(2): p. 145-156 DOI: https://doi.org/10.1016/S0168-3659(00)00243-1.

77. GombÁs, Á., P. Szabó-Révész, M. Kata, G. Regdon,E. István, *Quantitative Determination of Crystallinity of α-Lactose Monohydrate by DSC.* Journal of Thermal Analysis and Calorimetry, 2002. **68**: p. 503-510 DOI: 10.1023/A:1016039819247.

9. Bibliography

9.1. The publications on the subject of the thesis

1. Borbás B, Kállai-Szabó N, Lengyel M, Balogh E, Basa B, Süvegh K, Zelkó R, Antal I. Microfabrication of controlled release osmotic drug delivery systems assembled from designed elements. Expert Opinion On Drug Delivery. 2024; 21 (11)
IF: 5.4

2. Borbás B, Kohod Z, Kállai-Szabó N, Basa B, Lengyel M, Zelkó R, Antal I. Evaluation of 3D-Printed Balls with Photopolymer Resin as Grinding Medium Used to Alternatively Reduce Warmup During Dry Milling. Polymers. 2025; 17 (13)
IF: 4.9

9.2. Further publications

Basa B, Jakab G, Kállai-Szabó N, Borbás B, Fülöp V, Balogh E, Antal I. Evaluation of biodegradable PVA-based 3D printed carriers during dissolution. Materials. 2021; 14(6).
IF: 3,748

10. Acknowledgement

I would like to express my deepest gratitude to my supervisor, Prof. Dr. Antal István, who guided me throughout my whole research from the beginning as a TDK student to this moment. His vision, valuable insights and innovative ideas helped me a lot to evolve in the scientific field. I am also thankful for the opportunities he gave me during the years of mutual work.

I would also like to thank Dr Kállai-Szabó Nikolett, who was always there if I was struck and always supported me to be able to grow and improve. His valuable ideas contributed a lot to my research.

I am grateful to Prof. Dr. Zelkó Romána for her continuous help during my doctoral studies. I learnt a lot from her about the evaluation of results. Her professionalism towards the scientific publication work and her altruistic helpfulness helped me to a better scientist.

I would like to thank Dr. Bálint Basa for his guidance in the design and fabrication with 3D printing. Due to his valuable teaching, I became a better professional in the field.

I am grateful to my co-authors, Dr Bertalanné Balogh Emese, Dr Lengyel Miléna, Dr Kohod Zsófia, and Dr Károly Süvegh, for their valuable contribution to the research and for the preparation of the mutual publications.

I am thankful for Bánki-Horváthné Jakab Katalin, Csukás-Berta Nicolette, and Román Diána for the help they provided me in the measurements and in the educational matters. I am grateful to all colleagues and friends in the Department of Pharmaceutics for their help in scientific and educational tasks, and that they provided an exceptional atmosphere.

I am grateful to my wife, Dr. Borbás-Benyovszky Anna, my parents, Borbás Balázs and Borbásné Penke Judit and my brother, Borbás Levente, for their continuous and unconditional support. Thank you for standing by me in the most difficult times.